NASA TECHNICAL NOTE

NASA TN D-2925

NASA TN D-2925

MAXIMUM LIFT-DRAG-RATIO CHARACTERISTICS OF RECTANGULAR AND DELTA WINGS AT MACH 6.9

by Jim A. Penland

Langley Research Center

Langley Station, Hampton, Va.

NATIONAL AERONAUTICS AND SPACE ADMINISTRATION • WASHINGTON, D. C. • AUGUST 1965

NASA TN D-2925

MAXIMUM LIFT-DRAG-RATIO CHARACTERISTICS OF RECTANGULAR AND DELTA WINGS AT MACH 6.9

By Jim A. Penland

Langley Research Center
Langley Station, Hampton, Va.

NATIONAL AERONAUTICS AND SPACE ADMINISTRATION

For sale by the Clearinghouse for Federal Scientific and Technical Information
Springfield, Virginia 22151 – Price $2.00

MAXIMUM LIFT-DRAG-RATIO CHARACTERISTICS OF RECTANGULAR AND DELTA WINGS AT MACH 6.9

By Jim A. Penland
Langley Research Center

SUMMARY

A theoretical and experimental study of a variety of rectangular and delta planform wings at a Mach number of 6.9 and a range of root-chord Reynolds numbers from 0.35×10^6 to 4.1×10^6 has been made. This study shows that good predictions of $(L/D)_{max}$ are possible on rectangular wings but that the predicted $(L/D)_{max}$ for delta wings is approximately 10 percent higher than that for experiment.

Severe losses of $(L/D)_{max}$ occur with decreasing Reynolds number for all configurations and it may be inferred that $(L/D)_{max}$ values greater than about 3 will be difficult to attain at low Reynolds numbers (Reynolds numbers less than 0.1×10^6) on configurations having useful volume. The flat-bottom configuration shows the highest $(L/D)_{max}$ on simple shapes where no favorable interference can occur.

Thickness ratio and aspect ratio in that order are prime factors affecting $(L/D)_{max}$ irrespective of planform geometry. Within a family of shapes the optimum shape may be determined by use of a composite plot of aspect ratio, thickness ratio, volume-area ratio, and $(L/D)_{max}$. At a Mach number of 6.9 the curve of one-half the cotangent of the average angle of attack appears to form an upper boundary for both calculated and experimental values of $(L/D)_{max}$ for rectangular- and delta-wedge wings.

INTRODUCTION

In the hypersonic flight of vehicles capable of long-range cruise for transport, reconnaissance or bombing missions, and orbital boost gliders with global landing potential, the need for an efficient hypersonic configuration prevails. The maximum lift-drag ratio of a vehicle is, of course, indicative of its aerodynamic efficiency. Although some hypersonic data are available on various shapes (refs. 1 to 13), there are insufficient experimental or theoretical studies available in which the various geometric parameters are varied

through wide ranges to establish trends which point toward optimum configurations. Whether these vehicles will eventually take the form of a distinct wing-body shape, a blended wing-body, or a sophisticated lifting body is therefore, at present, an open question. To provide information on which an intelligent decision can be based, investigations of various shapes are currently underway at the NASA Langley Research Center. References 14 to 17 present results obtained in body-wing (half-cone delta wing) and lifting-body configurations. The present paper presents results of a theoretical and experimental investigation conducted to determine the effects of leading-edge sweep, thickness ratio, aspect ratio, volume, and Reynolds number on the maximum lift-drag ratio of sharp-leading-edge delta- and rectangular-wedge wings.

SYMBOLS

A aspect ratio

b wing span

c wing chord

c_r root chord of delta wing

$\bar{c}$ mean aerodynamic chord

C_A axial-force coefficient $\left(F_A - F_b\right)/q_\infty S_p$

C_D drag coefficient, $F_D'/q_\infty S_p$

C_F average skin-friction coefficient, $F_F/q_\infty S_p$

C_L lift coefficient, $F_L/q_\infty S_p$

C_m pitching-moment coefficient, $M_Y/q_\infty S_p \bar{c}$

C_N normal-force coefficient, $F_N/q_\infty S_p$

$C_{N,\infty}$ normal-force coefficient for $A = \infty$

F_A axial force

F_b base-pressure correction, $(p_\infty - p_b)S_b$

F_F average skin friction

$F_D' = F_N \sin \alpha + (F_A - F_b)\cos \alpha$

$F_L = F_N \cos \alpha + (F_b - F_A) \sin \alpha$

F_N	normal force
L/D	lift-drag ratio, C_L/C_D
$(L/D)_{max}$	maximum lift-drag ratio
M	free-stream Mach number
M_Y	pitching moment
p_b	base pressure
p_∞	free-stream static pressure
q_∞	free-stream dynamic pressure
R	free-stream Reynolds number based on maximum chord unless otherwise stated
S_b	base area of wing
S_p	planform area of wing
t	maximum thickness
V	total volume of wing
α	angle of attack, deg
α_{av}	average angle of attack, $\alpha - \frac{\theta}{2}$, deg
θ	wedge angle, deg
Λ	sweep angle of wing leading edge, deg

MODELS

Photographs of most of the models tested are shown in figure 1 and the geometric details of all models are presented in figure 2. These particular wedge wing models although of different planform have their entire volumes encompassed within the so-called shadow region at an angle of attack equal to $\tan^{-1} \frac{t}{c}$. The relationship of aspect ratio, volume, thickness ratio, and

leading-edge sweep angle for wedges is presented in appendix A. All models were machined from solid aluminum-alloy stock with care taken to maintain all leading edges as sharp as possible. Upon completion, these leading-edge radii were measured and found to be between 0.001 and 0.004 inch for all models.

APPARATUS, TESTS, AND DATA ACCURACY

The tests were conducted in the Mach number 6.86 test section of the Langley 11-inch hypersonic tunnel. The tunnel-wall boundary-layer thickness, and hence the free-stream Mach number of this test section, is dependent upon the stagnation pressure. For these tests, the stagnation pressure varied from 5 to 30 atmospheres and the minimum stagnation temperature used varied from 500° F to 620° F, respectively (to avoid air liquefaction). The resulting range of Mach numbers was about 6.7 to 6.9 and range of Reynolds numbers was 0.06×10^6 to 0.34×10^6 per inch. The absolute humidity was kept to less than 1.9×10^{-5} pounds of water per pound of dry air for all tests.

Three-component force data were obtained by use of a strain-gage balance through an angle-of-attack range of about -6° to 18°. The axial-force component was adjusted for differences between the measured base pressure and the free-stream static pressure. The difference between individual spanwise base-pressure readings was within the accuracy of the pressure-measuring instruments. The maximum root-mean-square (rms) values of the uncertainties in the measurement of the force and moment coefficients for the individual test points at $(L/D)_{max}$ as a result of the force-balance system which has an accuracy of ±0.5 percent full scale and the setting of angle of attack are presented as follows:

RMS values of uncertainties in	Model 1 at $R = 0.73 \times 10^6$	Model 5 at $R = 0.73 \times 10^6$
C_L	±0.003	±0.01
C_D	±0.001	±0.003
$(L/D)_{max}$	±0.191	±0.55
C_m	±0.0018	±0.0054

Errors in plotted values of $(L/D)_{max}$ should be less than those tabulated because of their having been read from faired curves. Data measured at higher Reynolds numbers will have proportionally smaller errors due to higher loading of the strain-gage force balance. The stagnation pressure was measured to an accuracy of ±1.5 inches of mercury, and angle of attack was set to an accuracy of ±0.20°. (See appendix B for a discussion of possible error due to inaccuracies in setting angle of attack.)

THEORY

The calculations of the inviscid longitudinal characteristics of the delta and rectangular wedge shapes presented in this report were made by shock-expansion theory using the oblique shock and Prandtl-Meyer expansion tables of reference 18. Estimates of laminar skin-friction coefficients were made by the methods of reference 19 which include the boundary-layer-displacement effects on the frictional drag component. Two types of tip correction were applied to the rectangular wings. The vertical side areas were corrected for viscous effects by assuming them to be delta wings for purposes of skin-friction calculation. Decreases in pressure coefficients near the tip due to finite aspect-ratio effects were accounted for by use of linear theory based on free-stream Mach angle as presented in reference 20.

The lift-drag ratio of high-efficiency bodies is strongly influenced by the effects of skin friction and its marked variations with Reynolds number. This influence is readily illustrated by calculating, for the zero-thickness flat plate, the change of lift-drag ratio with variations of Reynolds number and angle of attack. Figure 3 presents the results of such a calculation for both two-dimensional and delta-planform wings in laminar flow at a free-stream Mach number of 6.9. (Within the confines of the theory used herein, delta wings are unaffected by variations of aspect ratio.) As a limiting case (skin friction equal zero, corresponding to infinite Reynolds number), the curve of cot α is shown. These curves illustrate the severe decay of L/D throughout the angle-of-attack range with decreasing Reynolds number. The further decrease of L/D for the delta planform wings is due to the lower effective Reynolds number associated with shorter average chord. A significant trend showing that the $(L/D)_{max}$ occurs at successively lower angles of attack as the maximum value increases is important due to the correspondingly lower lift coefficients at $(L/D)_{max}$ and the decrease of the angle-of-attack range for high L/D. The locus of these points of $(L/D)_{max}$ for both the two-dimensional and delta-planform flat plates may be represented by the curve $(\cot \alpha)/2$, and thus represents a more reasonable limiting boundary for the case of skin friction greater than zero at hypersonic speeds. Since linearized theory shows that $(L/D)_{max} = 1/2\alpha$, this limiting curve is obtained by assuming $\alpha = \tan \alpha$. This boundary will be discussed in more detail subsequently.

The crossplot of $(L/D)_{max}$ with Reynolds number (inset of fig. 3) provides a summary of what may be expected within a very limited range of Reynolds numbers for flat-plate wings. The addition of aspect-ratio effects to the overall calculations of the two-dimensional shapes shows the losses to be expected for somewhat more realistic planforms. For a given Reynolds number based on vehicle length, a rectangular wing having an aspect ratio of 0.35 is only slightly better than a delta planform with its high viscous losses in the tip regions.

It is indicated from this theoretical study at $M = 6.9$ that losses in $(L/D)_{max}$ are to be expected with any decrease in Reynolds number. It may be further anticipated that losses in $(L/D)_{max}$ will increase with Mach number because of the rate of increase of boundary-layer-displacement effects (ref. 14).

RESULTS AND DISCUSSION

To show a comparison between theory and experiment throughout the angle-of-attack range, the results of four representative tests, two of rectangular wings (models 6 and 10) and two of roof delta wings (models 1 and 5) are presented in figure 4. These models have in common, aspect ratios of 1.07 (models 6 and 1) and 0.35 (models 10 and 5) and volume$^{2/3}$—planform-area ratios of 0.147 (models 6 and 1) and 0.210 (models 10 and 5). The thickness ratio of the rectangular wings was slightly greater than that of the delta wings due to the variation in geometry necessary to keep the previously mentioned parameters constant. (See appendix A for relationship of V, t/c, and Λ for wedge wings.)

Inspection of figure 4 shows that the quality of prediction varies with the model planform shape and the aspect ratio. Figure 4(a) shows that good predictions were possible for all longitudinal parameters for the A = 1.07 rectangular wedge, whereas figure 4(b) shows that a reduction of aspect ratio to 0.35 resulted in the underprediction of both lift and drag coefficients but that the prediction of $(L/D)_{max}$ was good. This good prediction was due in part to the use of flat-plate linear theory to correct for tip losses on shapes with a finite thickness ratio and resulted in the overcorrection of both lift and drag for pressure decreases behind the tip Mach lines. The tip effects on the rectangular model were not large for the aspect ratio of 1.07 as shown by the L/D curve (fig. 4(a)), calculated with no vertical-tip skin friction or loss in normal force due to Mach waves originating at the leading-edge tips. These tip losses become significant as the aspect ratio decreases. Figure 4(b) shows that the estimated loss in $(L/D)_{max}$ due to tip losses at A = 0.35 is about twice that for A = 1.07.

Figures 4(c) and (d) show that good lift and drag predictions were obtained for the delta wing having $\Lambda = 75^\circ$ but that the $(L/D)_{max}$ for both delta-wing wedges ($\Lambda = 75^\circ$ and 85°) was overpredicted by about 10 percent, and that the normal and lift coefficients for the delta wing having $\Lambda = 85^\circ$ were also overpredicted. The inability to predict $(L/D)_{max}$ for the delta-wing models is due primarily to the low prediction of axial force and drag coefficients for model 1 with $\Lambda = 75^\circ$ and, the overprediction of normal force due to early leading-edge shock detachment on model 5 with $\Lambda = 85^\circ$. In addition crossflow, which was not accounted for in the calculations, and transition which may have occurred at this Reynolds number (ref. 11) may be contributing factors.

The complete results of the wind-tunnel test program covering the models shown in figures 1 and 2 were considered too extensive to warrant reporting in detail in this paper and are therefore presented in tabulated form in table I. That portion of the data considered most rewarding, that is, $(L/D)_{max}$ for rectangular wings and for delta wings both upright and inverted, is presented and discussed subsequently.

Effect of Reynolds Number

The effect of Reynolds number variation on $(L/D)_{max}$ for several models having different thickness ratios and aspect ratios is presented in figure 5 for both rectangular and delta planform shapes. Losses in $(L/D)_{max}$ may be observed with decreasing Reynolds number for all configurations; the losses are largest for the shapes having the higher levels of $(L/D)_{max}$ and are relatively small for the configurations with lower efficiency.

Figure 5(a) also shows experimentally and theoretically that increasing the thickness ratio of a configuration to provide useful volume will result in a loss in $(L/D)_{max}$. (See appendix A for relationship of volume and thickness ratio.) The loss of $(L/D)_{max}$ with a decrease in aspect ratio for a nearly constant thickness ratio, due to increasing tip losses is evident from a comparison of models 6 and 10.

Figure 5(b) shows $(L/D)_{max}$ values for a series of delta wings through a range of Reynolds numbers for wings with both flat-bottom and flat-top orientations. This figure shows the overprediction of $(L/D)_{max}$ by theory, as discussed in figure 4, throughout the range of Reynolds numbers of the test. The predicted difference between the $(L/D)_{max}$ values for the flat-bottom and flat-top orientation was consistently less than that measured experimentally. Considerable scatter may be noted in the experimental data in this figure, due in part to the random nature of error always found in wind-tunnel measurements of $(L/D)_{max}$ and in part to transition that is to be expected at the higher Reynolds numbers. (See refs. 11 and 14.) In all tests of these sharp leading-edge delta-wing wedge models, the flat-bottom orientation gave the higher levels of $(L/D)_{max}$ as expected for simple shapes where no favorable interference occurs.

From these trends it may be inferred that high values of $(L/D)_{max}$ (greater than about 3) will be difficult to attain at low Reynolds numbers $(R < 0.1 \times 10^6)$ on configurations having useful volume. Additional losses in L/D may be incurred due to trim control and base drag under flight conditions.

Effect of Volume Parameter on $(L/D)_{max}$

Figure 6(a) presents a plot of $(L/D)_{max}$ against the nondimensional volume parameter $V^{2/3}/S_p$ for several rectangular wings having aspect ratios of 0.35 and about 1.0 at a constant Reynolds number of 1.5×10^6 (some data adjusted to 1.5×10^6) and Mach number of 6.9. These rectangular wings exhibit good agreement with theory and, as expected, a considerable loss of $(L/D)_{max}$ with increasing $V^{2/3}/S_p$. It should be noted that in the more useful volume region $V^{2/3}/S_p > 0.1$ some increases in volume ratio may be gained by decreasing the aspect ratio at constant thickness ratio with little loss in $(L/D)_{max}$.

Conversely for a constant $V^{2/3}/S_p$, the $(L/D)_{max}$ may be increased by decreasing the aspect ratio. At extremely low values of $V^{2/3}/S_p$ and thickness ratio, the theory indicates that increases in aspect ratio may be expected to improve $(L/D)_{max}$ values, but configurations of this nature may be of very limited practical use.

Figure 6(b) presents data and theory for a series of roof delta wings for $R = 1.5 \times 10^6$ and $M = 6.9$. The data shown in this figure are for flat-bottom orientation; as discussed previously, the flat-top orientation gave lower values of $(L/D)_{max}$ for all tests. Agreement of experiment and theory is in trend only with the experimental data consistently being about 10-percent low. With respect to variations of $(L/D)_{max}$ with aspect ratio, thickness ratio, and volume ratio, the trends are identical with those for rectangular wings in the useful volume region $\left(\text{i.e., } V^{2/3}/S_p > 0.1\right)$. For both rectangular and delta wings the thickness ratio appears to be the dominate geometric parameter with sweep and/or the aspect ratio having a secondary effect. At levels of $V^{2/3}/S_p < 0.1$ the delta wing theoretical curves converge into a single line which indicates that variations of sweep and/or aspect ratio may be expected to contribute little change in $(L/D)_{max}$.

Effect of Thickness Ratio

Figure 7 presents the results of tests and calculations for a series of rectangular- and roof-delta-wedge wings with $A \approx 1$ at a Reynolds number of 0.98×10^6 and 1.33×10^6, respectively, and a Mach number of 6.9. For this study the thickness ratio was allowed to vary up to a maximum of 0.3, and due to the constant aspect ratio used, the $V^{2/3}/S_p$ varied also. (See inset plot.) The loss in $(L/D)_{max}$ amounts to approximately 50 percent within this range of thickness ratios and graphically illustrates the serious losses that occur due to increasing volume by increasing t/c. The major reason for this loss is a nine-fold increase in minimum drag and less than a three-fold increase in the slope of the normal-force curve as t/c varies from 0 to 0.3. The importance of minimum drag in the attainment of $(L/D)_{max}$ should not be underestimated. Theoretical methods based on linear theory have shown that $(L/D)_{max}$ can be expressed in terms of minimum drag and lift-curve slope (ref. 11). Furthermore, reference 21 shows that for symmetrical configurations in Newtonian flow that the lift-curve slope can be expressed in terms of minimum drag. It may therefore be inferred from both experimental and theoretical studies for symmetrical shapes at hypersonic speeds that minimum drag is of primary importance in the attainment of $(L/D)_{max}$.

It has often been suspected that filling in the shadow region would have little or no effect on L/D. Since the angle of attack at which $(L/D)_{max}$ was measured for these configurations was in excess of that needed to shield the

total body volume (except for the model with $t/c = 0.3$) within the shadow region, this effect can be examined. To show the magnitude of this effect, a curve showing L/D of a flat plate at an angle of attack equal to the angle of attack of the lower surface of each model at $(L/D)_{max}$ is included in figure 7. The difference between this curve and the one labeled "with tip correction" indicates the penalty in L/D due to filling in the shadow region. This loss is significant and amounts to as much as 10 percent (for the models having the larger t/c values).

Effect of Aspect Ratio

The effect of aspect ratio on $(L/D)_{max}$ of both rectangular and delta planform wedges has been discussed briefly in the presentation of figures 6(a) and (b). A more detailed study in which aspect ratio was varied for a constant $V^{2/3}/S_p$ ratio is presented in figure 8 for constant Reynolds numbers, based on both the root chord and on the square root of the planform area. This latter case is included to show the behavior when planform area is held constant. Experimental data in both figures 8(a) and 8(b) show peak values of $(L/D)_{max}$ at $A \approx 0.3$ to 0.4; both the peak values and the aspect ratio at which they occur are dependent on Reynolds number, thus indicating optimum shapes for the fixed $V^{2/3}/S_p$ ratio of 0.20. Curves shown in figure 8(a) with no correction for tip losses show no optimum, but with the addition of the tip loss due to skin friction on the vertical side areas of the rectangular wings an optimum is approached that does not compare with the measured data. Full correction for tip losses due to changes in the local pressure behind the Mach lines emanating from the leading-edge tips and for skin friction along the vertical side areas was applied to the curves shown in figure 8(b) and good predictions of $(L/D)_{max}$ resulted. As the losses of normal force due to local pressure variation are a function of both aspect ratio and Mach number, an inset plot is provided to show their magnitude. The small sketches across the bottom of the figure show the areas affected for various aspect ratios at the stream Mach number of 6.9. During this study it was necessary to vary the thickness ratio with aspect ratio in order that $V^{2/3}/S_p$ be constant. For the case of constant planform area $(R = 0.61 \times 10^6)$, the optimum performance is reached when the losses due to tip effects balance the gains made by decreasing the thickness ratio and aspect ratio, which increases the chord and reduces the skin-friction coefficient. For the constant root-chord case $(R = 0.64 \times 10^6)$ the gains of $(L/D)_{max}$ with decreasing aspect ratio may be attributed solely to the accompanying decrease in thickness ratio, which are balanced by the increasing tip losses. The optimum $(L/D)_{max}$ occurred at different aspect ratios depending on the flow conditions and it would be expected that for other classes of configurations similar optimums would occur.

Summary of Theoretical Wing Characteristics and Optimum Configurations

It has been shown that $(L/D)_{max}$ for rectangular wings can be calculated with good accuracy throughout a range of Reynolds numbers and for various aspect ratios and thickness ratios, and that the trends of $(L/D)_{max}$ for delta wings may be calculated, but the calculated values of $(L/D)_{max}$ are approximately 10-percent higher than for experimental data. For a given Reynolds number, calculations showing the overall relationship of aspect ratio or sweep, thickness ratio, volume ratio, and maximum lift-drag ratio are presented in figure 9 for a wide range of rectangular and delta wings. This figure shows the predominate effect of thickness ratio in the attainment of high $(L/D)_{max}$ and the secondary effect of aspect ratio except at very low thickness ratios and aspect ratios. Also shown is the reduction in $(L/D)_{max}$ as $V^{2/3}/S_p$ increases as discussed previously. As the aspect ratio is reduced below about 1 or the sweep angle increased beyond about 80° the curves of constant $(L/D)_{max}$ take a decided turn toward the region of lower thickness ratio. This increased curvature of the $(L/D)_{max}$ curves combined with the superimposed lines of constant $V^{2/3}/S_p$ make possible the determination of the optimum configuration with regard to $(L/D)_{max}$ for these geometric parameters. This optimum occurs at the point of tangency between the curves of $(L/D)_{max}$ and those of $V^{2/3}/S_p$ which is shown by a shaded band. An optimum configuration having high $V^{2/3}/S_p$ may be seen to have a low aspect ratio or high sweep and a relatively large thickness ratio and low $(L/D)_{max}$, whereas a high $(L/D)_{max}$ shape is characterized by higher aspect ratio or lower sweep and lower thickness and volume ratios. The curves of figure 9 therefore represent the optimized solution for rectangular and delta planform wings with the Mach number, Reynolds number, and volume parameter as the restrictive conditions. Other restrictive conditions, of course, can result in different optimum shapes. The difference due to a decrease in Reynolds number from 1.5×10^6 to 0.64×10^6 on rectangular wings for a constant $V^{2/3}/S_p = 0.2$ may be seen by comparing figures 8(b) and 9(a). If $V^{2/3}/\text{wetted area}$ is used in place of $V^{2/3}/S_p$, however, the difference in optimum configurations is not great. For example, the optimum $(L/D)_{max} = 6$ rectangular wing using $V^{2/3}/\text{wetted area}$ has $A = 0.53$ and $t/c = 0.85$ whereas using $V^{2/3}/S_p$ results in a wing having $A = 0.47$ and $t/c = 0.8$.

Comparison of Delta and Rectangular Planform Wedge Wings

To this point the discussion has dealt with delta and rectangular wings as separate shapes; figure 10 compares the two wings based on a common Reynolds number, constant aspect ratios, and constant $V^{2/3}/S_p$ ratios. Interpolated

data from figure 5 were used to compile this plot. For the case where the Reynolds number for both wings is based on a constant root chord ($R = 0.74 \times 10^6$), the rectangular wings exhibit the highest $(L/D)_{max}$ and the delta wings, the lowest because of the high viscous losses in the tip region of the deltas where the local chord is small and the local Reynolds numbers are low. Reference 19 indicates that for equivalent viscous effects on flat-plate delta and rectangular wings that the root-chord Reynolds number on the delta wing should be larger by factor of 1.777 than the Reynolds number on the rectangular wing. Data are shown for this case in figure 10 for $R = 1.32 \times 10^6$ based on this ratio and it may be seen that the $(L/D)_{max}$ values for the delta wings are slightly higher than those for the rectangular wings. This condition might be anticipated as the tip losses on the rectangles would tend to reduce the $(L/D)_{max}$ values somewhat. If the configurations under consideration are assumed to have equal planform areas and the same average test Reynolds number, the delta wings must operate at a Reynolds number of 1.48×10^6 to compare with the rectangular wings operating at 0.74×10^6. On this basis also the data in figure 10 show the delta configurations to be superior to the rectangular shapes.

Correlation of Maximum Lift-Drag Ratios

In the discussion entitled "Theory" it was pointed out that the calculated $(L/D)_{max}$ of zero-thickness flat plates could be approximated very closely by using the linearized theory curve $(\cot \alpha)/2$. A futher analysis shows that if an average angle of attack is used, that is, the angle measured from the relative wind to the model mean line, $(L/D)_{max}$ of configurations of various planforms at various Reynolds numbers having finite thickness can also be correlated by using functions of the $\cot \alpha$ curve. The results of this investigation, both theoretical and experimental, are shown in figure 11. This figure shows that nearly all values of $(L/D)_{max}$ whether measured or calculated fall beneath the $\frac{\cot \alpha_{av}}{2}$ curve, thus establishing an upper limit of $(L/D)_{max}$ for simple wedge configurations at a hypersonic Mach number.

CONCLUSIONS

Analysis of experimental data using the shock-expansion theory on a variety of rectangular and delta planform wings at a Mach number of 6.9 and a range of Reynolds numbers from 0.35×10^6 to 4.1×10^6 leads to the following conclusions.

1. Good predictions of maximum lift-drag ratios $(L/D)_{max}$ were possible on the rectangular planform wings, whereas the $(L/D)_{max}$ values were overpredicted by about 10 percent on the delta planform wings.

2. A severe decay of maximum lift-drag ratio occurs with decreasing Reynolds numbers for all configurations. It may be inferred that high values of $(L/D)_{max}$ (greater than about 3) will be difficult to attain at low Reynolds numbers (Reynolds numbers less than 0.1×10^6) on configurations having useful volume.

3. The flat-bottom-orientated delta models exhibited the superior maximum lift-drag ratios as predicted by theory on simple configurations where no favorable interference effects occur.

4. At hypersonic speed where tip losses are relatively small, maximum lift-drag ratio appears to be primarily a function of thickness ratio and secondarily a function of aspect ratio. This is due to a disproportionate increase in minimum drag in relation to lift-curve slope irrespective of planform geometry. The determination of optimum shapes is possible by construction of a composite plot of aspect ratio, thickness ratio, $\text{volume}^{2/3}$—planform-area ratio, and maximum lift-curve slope.

5. At the hypersonic Mach number of 6.9 the curve of one-half the cotangent of the average angle of attack, that is, the angle measured from the relative wind to the model mean line, forms an upper boundary for both calculated and experimental values of maximum lift-drag ratio for rectangular and delta wedges. This limiting boundary may be readily derived by using linearized theory.

Langley Research Center,
National Aeronautics and Space Administration,
Langley Station, Hampton, Va., May 3, 1965.

APPENDIX A

GEOMETRY OF RECTANGULAR AND DELTA WEDGE WINGS

In any discussion concerning the useful volume of an aerodynamic shape it is appropriate to see how the volume varies with changes in the configuration geometry. The relatively widespread use of the nondimensional ratio of volume$^{2/3}$ to the planform area as an efficiency correlating parameter further complicates the issue and makes separation of the effects of shape variables difficult. Figures 12(a) and (b) presents the relationship of volume and volume$^{2/3}$/area ratio to thickness ratio and aspect ratio for rectangular- and delta-wedge wings. The volume increases linearly with either an increase in thickness ratio or aspect ratio; the volume$^{2/3}$/area ratio, however increases with thickness ratio but decreases with increasing aspect ratio.

For delta wings the aspect ratio may be expressed in terms of sweep angle which results in $A = 4 \cot \Lambda$. A plot of this relation is presented in figure 12(c) and shows that the aspect ratio for delta wings is relatively insensitive to sweep angle at the large values of sweep under consideration for hypersonic configurations, therefore yielding only small difference in aspect ratio for sizable variations of sweep angle.

APPENDIX B

LIFT-DRAG RATIO AND ANGLE OF ATTACK

The majority of wind tunnels obtain lift-drag ratios on a model by measuring the normal and axial forces through an angle-of-attack range and calculating the lift and drag parameters from the test results.

The sensitivity of lift-drag ratio to any deviation from the assumed angle of attack is appreciable, and at the higher values of L/D a considerable error may occur for a relatively small variation in angle of attack. This geometric problem can be shown readily through the use of the equations involving lift, drag, normal and axial forces, and angle of attack which when combined result in the following relation:

$$L/D = \frac{C_N/C_A \cot \alpha - 1}{\cot \alpha + C_N/C_A}$$

which shows that the lift-drag ratio is dependent only on the normal-to-axial-force ratio and the angle of attack. A plot of this relationship is presented in figure 13 where it may be seen that the sensitivity of L/D to variation in assumed angle of attack varies not only with the level of L/D but also with the angle-of-attack region in question. Generally however the higher the level of L/D the more serious the deviation of the angle of attack. For example, at $L/D = 2.0$ an error of $\pm 1^{\circ}$ results in only about ± 0.1 error in L/D; at $L/D = 7$ however, an error of $\pm 1^{\circ}$ can result in nearly ± 1.0 error in L/D.

REFERENCES

1. Bertram, Mitchel H.; and McCauley, William D.: Investigation of the Aerodynamic Characteristics at High Supersonic Mach Numbers of a Family of Delta Wings Having Double-Wedge Sections With the Maximum Thickness at 0.18 Chord. NACA RM L54G28, 1954.

2. Bertram, Mitchel H.; and McCauley, William D.: An Investigation of the Aerodynamic Characteristics of Thin Delta Wings With a Symmetrical Double-Wedge Section at a Mach Number of 6.9. NACA RM L55B14, 1955.

3. McLellan, Charles H.; and Dunning, Robert W.: Factors Affecting the Maximum Lift-Drag Ratio at High Supersonic Speeds. NACA RM L55L20a, 1956.

4. Eggers, A. J., Jr.; and Syvertson, Clarence A.: Aircraft Configurations Developing High Lift-Drag Ratios at High Supersonic Speeds. NACA RM A55L05, 1956.

5. Syvertson, Clarence A.; Wong, Thomas J.; and Gloria, Hermilo R.: Additional Experiments With Flat-Top Wing-Body Combinations at High Supersonic Speeds. NACA RM A56I11, 1957.

6. McLellan, Charles H.; Bertram, Mitchel H.; and Moore, John A.: An Investigation of Four Wings of Square Planform at a Mach Number of 6.9 in the Langley 11-Inch Hypersonic Tunnel. NACA Rept. 1310, 1957. (Supersedes NACA RM L51D17.)

7. Syvertson, Clarence A.; Gloria, Hermilo R.; and Sarabia, Michael F.: Aerodynamic Performance and Static Stability and Control of Flat-Top Hypersonic Gliders at Mach Numbers From 0.6 to 18. NACA RM A58G17, 1958.

8. Armstrong, William O.; and Ladson, Charles L. (with Appendix A by Donald L. Baradell and Thomas A. Blackstock): Effects of Variation in Body Orientation and Wing and Body Geometry on Lift-Drag Characteristics of a Series of Wing-Body Combinations at Mach Numbers From 3 to 18. NASA TM X-73, 1959.

9. McLellan, Charles H.; and Ladson, Charles L.: A Summary of the Aerodynamic Performance of Hypersonic Gliders. NASA TM X-237, 1960.

10. Geiger, Richard E.: Experimental Lift and Drag of a Series of Glide Configurations at Mach Numbers of 12.6 and 17.5. J. Aerospace Sci., vol. 29, no. 4, Apr. 1962, pp. 410-419.

11. Bertram, Mitchel H.; Fetterman, David E., Jr.; and Henry, John R.: The Aerodynamics of Hypersonic Cruising and Boost Vehicles. Proceedings of the NASA-University Conference on the Science and Technology of Space Exploration, Vol. 2, NASA SP-11, 1962, pp. 215-234. (Also available as NASA SP-23.)

12. Goebel, T. P.; Martin, J. J.; and Boyd, J. A.: Factors Affecting Lift-Drag Ratios at Mach Numbers From 5 to 20. AIAA J., vol. 1, no. 3, Mar. 1963, pp. 640-650.

13. Blackstock, Thomas A.; and Ladson, Charles L.: Comparison of the Hypersonic Aerodynamic Characteristics of Some Simple Winged Shapes in Air and Helium. NASA TN D-2328, 1964.

14. Becker, John V.: Studies of High Lift/Drag Ratio Hypersonic Configurations. International Council of the Aeronautical Sciences, Fourth Congress, Paris - 1964, Spartan and MacMillan & Co., Ltd., 1965.

15. Johnston, Patrick J.; Snyder, Curtis D.; and Witcofski, Robert D.: Maximum Lift-Drag Ratios of Delta-Wing—Half-Cone Combinations at a Mach Number of 20 in Helium. NASA TN D-2762, 1965.

16. Fetterman, David E.; Henderson, Arthur, Jr.; Bertram, Mitchel H.; and Johnston, Patrick J.: Studies Relating to the Attainment of High Lift-Drag Ratios at Hypersonic Speeds. NASA TN D-2956, 1965.

17. Fetterman, David E.: Favorable Interference Effects on Maximum Lift-Drag Ratios of Half-Cone Delta-Wing Configurations at Mach 6.86. NASA TN D-2942, 1965.

18. Malvestuto, Frank S., Jr.; Sullivan, Phillip J.; Marcy, Williams L.; Mortzschky, Herbert A.; Larrivee, Jules A.; and Huggins, Vivan E.: Study to Determine Aerodynamic Characteristics on Hypersonic Re-Entry Configurations. Part II - Analytical Phase, Volume 2 - Design Charts. WADD-TR-61-56, Pt. II, Vol. 2 (AD 28 6890), U.S. Air Force, Aug. 1962.

19. Bertram, Mitchel H.: Boundary-Layer Displacement Effects in Air at Mach Numbers of 6.8 and 9.6. NASA TR R-22, 1959. (Supersedes NACA TN 4133.)

20. Liepmann, H. W.; and Roshko, A.: Elements of Gasdynamics. John Wiley & Sons, Inc., c.1957.

21. Chapman, Gary T.: A Simple Relationship Between the Drag Near Zero Lift and the Initial Normal-Force-Curve Slope Obtained From Newtonian Theory. AIAA J. (Tech. Notes), vol. 3, no. 6, June 1965, pp. 1194-1195.

TABLE I.- TABULATION OF DATA

(a) Model 1

$R = 0.62 \times 10^6$			
α, deg	C_N	C_A	C_m
14.00	0.1807	0.0047	0.0018
12.00	.1431	.0058	.0019
10.00	.1111	.0073	.0013
8.00	.0778	.0075	.0011
6.00	.0474	.0089	.0009
4.00	.0194	.0106	.0004
2.00	-.0068	.0120	.0001
.00	-.0332	.0133	-.0004
-2.00	-.0640	.0142	.0013

$R = 0.78 \times 10^6$			
α, deg	C_N	C_A	C_m
14.00	0.1826	0.0043	0.0015
12.00	.1513	.0053	.0016
10.00	.1145	.0058	.0018
8.00	.0837	.0059	.0003
6.00	.0518	.0071	.0005
4.00	.0259	.0085	.0001
2.00	-.0064	.0092	-.0002
.00	-.0317	.0109	-.0006
-2.00	-.0567	.0129	-.0008
-5.00	-.0985	.0155	-.0009

$R = 1.39 \times 10^6$			
α, deg	C_N	C_A	C_m
14.00	0.1790	0.0031	0.0011
12.00	.1443	.0036	.0008
10.00	.1109	.0039	.0004
8.00	.0784	.0044	.0008
6.00	.0474	.0052	.0005
4.00	.0206	.0062	.0002
2.00	-.0083	.0079	.0004
.00	-.0310	.0093	-.0003
-2.00	-.0630	.0114	-.0001
-4.00	-.0906	.0134	-.0006

$R = 2.81 \times 10^6$			
α, deg	C_N	C_A	C_m
14.00	0.1873	0.0022	0.0008
12.00	.1554	.0035	.0009
10.00	.1173	.0030	.0006
8.00	.0891	.0035	.0006
6.00	.0567	.0041	.0006
4.00	.0242	.0052	.0003
2.00	-.0011	.0066	.0001
.00	-.0322	.0082	.0000
-2.00	-.0594	.0098	-.0001
-5.00	-.0974	.0136	-.0005

$R = 3.88 \times 10^6$			
α, deg	C_N	C_A	C_m
12.00	0.1520	0.0026	0.0009
10.00	.1191	.0025	.0004
8.00	.0842	.0028	.0003
6.00	.0511	.0037	.0003
4.00	.0219	.0049	.0001
2.00	-.0078	.0062	-.0001
.00	-.0347	.0079	-.0003
-2.00	-.0620	.0098	-.0006
-4.00	-.0874	.0119	-.0006

TABLE I.- TABULATION OF DATA - Continued

(b) Model 2

$R = 0.72 \times 10^6$			
α, deg	C_N	C_A	C_m
14.00	0.1690	0.0037	0.0013
12.00	.1349	.0051	.0017
10.00	.1060	.0058	.0008
8.00	.0752	.0061	.0003
6.00	.0472	.0069	.0003
4.00	.0245	.0086	-.0007
2.00	-.0023	.0084	.0003
.00	-.0264	.0086	-.0009
-2.00	-.0460	.0107	-.0007
-5.00	-.0790	.0126	-.0007

$R = 1.27 \times 10^6$			
α, deg	C_N	C_A	C_m
14.00	0.1676	0.0031	0.0004
12.00	.1366	.0036	.0002
10.00	.1076	.0045	.0003
8.00	.0742	.0052	-.0002
6.00	.0465	.0053	-.0002
4.00	.0224	.0065	-.0005
2.00	-.0026	.0072	-.0006
.00	-.0251	.0075	-.0006
-2.00	-.0478	.0087	-.0008
-5.00	-.0795	.0109	-.0006

$R = 1.41 \times 10^6$			
α, deg	C_N	C_A	C_m
14.00	0.1677	0.0025	0.0003
12.00	.1337	.0030	.0002
10.00	.1003	.0036	-.0001
8.00	.0715	.0043	.0000
6.00	.0446	.0053	.0000
4.00	.0198	.0064	-.0002
2.00	-.0038	.0074	-.0002
.00	-.0239	.0078	-.0009
-2.00	-.0487	.0085	-.0012
-4.00	-.0728	.0103	-.0009

$R = 2.54 \times 10^6$			
α, deg	C_N	C_A	C_m
14.00	0.1769	0.0015	0.0001
12.00	.1421	.0018	-.0001
10.00	.1127	.0023	.0001
8.00	.0807	.0028	.0002
6.00	.0510	.0037	-.0002
4.00	.0256	.0050	-.0001
2.00	-.0017	.0063	-.0007
.00	-.0256	.0070	-.0005
-2.00	-.0470	.0082	-.0004
-5.00	-.0800	.0109	-.0006

$R = 4.13 \times 10^6$			
α, deg	C_N	C_A	C_m
14.00	0.1761	0.0008	-0.0004
12.00	.1395	.0010	-.0003
10.00	.1077	.0014	-.0005
8.00	.0758	.0021	-.0004
6.00	.0477	.0030	-.0005
4.00	.0191	.0042	-.0006
2.00	-.0052	.0055	-.0007
.00	-.0266	.0064	-.0008
-2.00	-.0520	.0080	-.0009
-4.00	-.0736	.0099	-.0010

TABLE I.- TABULATION OF DATA - Continued

(c) Model 3

$R = 0.72 \times 10^6$

α, deg	C_N	C_A	C_m
14.00	0.1711	0.0095	0.0011
12.00	.1304	.0103	.0013
10.00	.0933	.0117	.0008
8.00	.0596	.0140	.0011
6.00	.0301	.0159	.0008
4.00	-.0007	.0184	.0004
2.00	-.0357	.0206	.0002
.00	-.0623	.0224	-.0003
-2.00	-.0896	.0257	-.0006
-5.00	-.1316	.0321	-.0009

$R = 1.36 \times 10^6$

α, deg	C_N	C_A	C_m
14.00	0.1735	0.0059	-0.0001
12.00	.1315	.0067	.0005
10.00	.0946	.0082	.0002
8.00	.0580	.0099	-.0002
6.00	.0277	.0123	.0003
4.00	-.0018	.0144	.0001
2.00	-.0372	.0170	.0000
.00	-.0643	.0202	-.0003
-2.00	-.0933	.0237	-.0006
-5.00	-.1359	.0302	-.0003

$R = 1.39 \times 10^6$

α, deg	C_N	C_A	C_m
14.00	0.1691	0.0046	0.0005
12.00	.1295	.0061	.0001
10.00	.0932	.0075	.0006
8.00	.0576	.0095	.0006
6.00	.0242	.0119	.0003
4.00	-.0096	.0145	.0002
2.00	-.0381	.0172	.0002
.00	-.0654	.0205	.0000
-2.00	-.1002	.0244	-.0002
-4.00	-.1295	.0286	-.0002

$R = 2.64 \times 10^6$

α, deg	C_N	C_A	C_m
14.00	0.1797	0.0038	-0.0008
12.00	.1378	.0052	-.0006
10.00	.0986	.0064	-.0005
8.00	.0624	.0082	-.0003
6.00	.0262	.0104	-.0001
4.00	-.0079	.0132	-.0002
2.00	-.0398	.0159	-.0002
.00	-.0675	.0189	-.0003
-2.00	-.0983	.0227	-.0003

$R = 3.90 \times 10^6$

α, deg	C_N	C_A	C_m
12.00	0.1348	0.0044	-0.0002
8.00	.0613	.0075	.0000
6.00	.0246	.0098	.0000
4.00	-.0103	.0124	-.0001
2.00	-.0392	.0151	-.0003
.00	-.0665	.0180	-.0004
-2.00	-.0991	.0199	-.0007

TABLE I.- TABULATION OF DATA - Continued

(d) Model 4

R = 0.71 × 10^6			
α, deg	C_N	C_A	C_m
14.00	0.1549	0.0064	0.0006
12.00	.1182	.0075	-.0008
10.00	.0853	.0090	.0000
8.00	.0525	.0107	-.0002
6.00	.0256	.0133	-.0002
4.00	-.0002	.0150	.0005
2.00	-.0246	.0163	.0001
.00	-.0507	.0189	.0009
-2.00	-.0756	.0214	-.0007
-4.00	-.0999	.0254	.0005

R = 0.72 × 10^6			
α, deg	C_N	C_A	C_m
14.00	0.1560	0.0071	0.0003
12.00	.1178	.0085	.0006
10.00	.0850	.0095	.0003
8.00	.0548	.0111	-.0002
6.00	.0283	.0131	.0002
4.00	.0012	.0146	.0000
2.00	-.0251	.0159	-.0003
.00	-.0465	.0171	-.0003
-2.00	-.0686	.0202	-.0009

R = 1.25 × 10^6			
α, deg	C_N	C_A	C_m
14.00	0.1579	0.0049	0.0003
12.00	.1174	.0057	.0002
10.00	.0883	.0076	.0002
8.00	.0563	.0085	.0001
6.00	.0282	.0103	-.0002
4.00	.0025	.0125	.0001
2.00	-.0245	.0141	-.0001
.00	-.0462	.0162	-.0001
-2.00	-.0682	.0188	.0000
-5.00	-.1061	.0241	-.0002

R = 1.40 × 10^6			
α, deg	C_N	C_A	C_m
14.00	0.1551	0.0037	-0.0001
12.00	.1156	.0050	.0000
10.00	.0839	.0066	.0004
8.00	.0523	.0079	.0002
6.00	.0239	.0097	-.0004
4.00	-.0031	.0119	.0000
2.00	-.0263	.0133	.0001
.00	-.0474	.0153	-.0001

R = 2.63 × 10^6			
α, deg	C_N	C_A	C_m
14.00	0.1632	0.0033	-0.0005
12.00	.1218	.0041	-.0003
10.00	.0922	.0054	-.0002
8.00	.0587	.0072	.0000
6.00	.0303	.0093	.0001
4.00	.0036	.0114	-.0001
2.00	-.0261	.0126	.0000
.00	-.0496	.0146	.0000
-2.00	-.0714	.0178	.0000
-5.00	-.1089	.0240	.0004

R = 3.98 × 10^6			
α, deg	C_N	C_A	C_m
14.00	0.1650	0.0021	-0.0013
12.00	.1285	.0032	-.0010
10.00	.0928	.0045	-.0007
8.00	.0577	.0062	-.0005
6.00	.0286	.0083	-.0005
4.00	.0012	.0103	-.0004
2.00	-.0262	.0122	-.0004
.00	-.0494	.0140	-.0004
-2.00	-.0757	.0173	-.0003
-4.00	-.0998	.0212	-.0002

TABLE I.- TABULATION OF DATA - Continued

(e) Model 5

$R = 0.66 \times 10^6$			
α, deg	C_N	C_A	C_m
14.00	0.1491	0.0060	0.0004
12.00	.1150	.0054	-.0029
10.00	.0877	.0079	-.0012
8.00	.0616	.0065	-.0016
6.00	.0355	.0092	-.0033
4.00	.0173	.0091	.0001
2.00	.0016	.0090	-.0009
.00	-.0145	.0108	.0008
-2.00	-.0324	.0108	-.0015

$R = 1.38 \times 10^6$			
α, deg	C_N	C_A	C_m
14.00	0.1493	0.0029	-0.0008
12.00	.1198	.0038	-.0009
10.00	.0932	.0042	-.0009
8.00	.0623	.0051	-.0008
6.00	.0394	.0040	-.0003
4.00	.0198	.0051	-.0003
2.00	.0008	.0050	.0000
.00	-.0143	.0049	-.0006
-2.00	-.0279	.0069	-.0010
-5.00	-.0528	.0099	.0001

$R = 1.40 \times 10^6$			
α, deg	C_N	C_A	C_m
14.00	0.1520	0.0015	-0.0002
12.00	.1145	.0025	.0005
10.00	.0860	.0030	-.0016
8.00	.0584	.0036	.0008
6.00	.0355	.0042	-.0002
4.00	.0139	.0048	-.0014
2.00	-.0008	.0059	.0001
.00	-.0164	.0046	.0001
-4.00	-.0469	.0086	.0001

$R = 2.67 \times 10^6$			
α, deg	C_N	C_A	C_m
14.00	0.1554	0.0004	-0.0005
12.00	.1278	.0015	-.0008
10.00	.0964	.0023	-.0004
8.00	.0662	.0028	-.0002
6.00	.0412	.0036	-.0005
4.00	.0216	.0042	-.0007
2.00	.0018	.0046	-.0004
.00	-.0145	.0046	-.0002
-2.00	-.0291	.0064	-.0007
-5.00	-.0548	.0085	-.0003

$R = 4.07 \times 10^6$			
α, deg	C_N	C_A	C_m
10.00	0.0920	0.0006	-0.0013
8.00	.0624	.0014	-.0011
6.00	.0378	.0024	-.0009
4.00	.0174	.0035	-.0007
2.00	.0000	.0046	-.0006
.00	-.0156	.0046	-.0005
-2.00	-.0312	.0062	-.0006
-4.00	-.0494	.0078	-.0008

TABLE I.- TABULATION OF DATA - Continued

(f) Model 6

R = 0.68 × 10^6			
α, deg	C_N	C_A	C_m
14.00	0.1874	0.0028	0.0021
12.00	.1476	.0035	.0012
10.00	.1079	.0038	.0013
9.00	.0890	.0043	.0011
8.00	.0726	.0051	.0011
6.00	.0384	.0066	-.0010
4.00	.0108	.0082	.0005
2.00	-.0197	.0106	.0002
.00	-.0518	.0129	.0002

R = 0.99 × 10^6			
α, deg	C_N	C_A	C_m
12.00	0.1535	0.0010	0.0007
10.00	.1140	.0023	.0002
8.00	.0768	.0038	.0001
6.00	.0433	.0056	.0004
4.00	.0130	.0079	-.0002

(g) Model 7

R = 0.70 × 10^6			
α, deg	C_N	C_A	C_m
18.00	0.2941	0.0022	0.0042
16.00	.2478	.0031	.0029
14.00	.1962	.0032	.0019
12.00	.1514	.0036	.0019
10.00	.1107	.0050	.0015
8.00	.0797	.0058	.0012
6.00	.0416	.0070	.0005
4.00	.0112	.0088	-.0002
2.00	-.0211	.0115	-.0001
.00	-.0480	.0141	-.0027

(h) Model 8

R = 0.66 × 10^6			
α, deg	C_N	C_A	C_m
20.00	0.3243	-0.0002	0.0028
18.00	.2757	.0018	.0018
16.00	.2198	.0039	.0011
14.00	.1679	.0055	.0005
12.00	.1310	.0085	.0007
10.00	.0788	.0122	.0004
4.00	-.0534	.0287	.0011
.00	-.1408	.0459	.0032

R = 1.47 × 10^6			
α, deg	C_N	C_A	C_m
18.00	0.2702	0.0009	0.0020
16.00	.2170	.0018	.0017
14.00	.1666	.0034	.0011
12.00	.1151	.0060	.0012
10.00	.0724	.0089	.0010
8.00	.0245	.0135	.0013
6.00	-.0193	.0190	.0011

TABLE I.- TABULATION OF DATA - Continued

(i) Model 9

R = 0.63 × 10^6			
α, deg	C_N	C_A	C_m
20.00	0.3145	0.0030	0.0035
18.00	.2588	.0052	.0032
16.00	.2060	.0070	.0033
14.00	.1657	.0081	.0019
12.00	.1188	.0114	.0016
10.00	.0782	.0150	.0018
8.00	.0298	.0183	.0012
4.00	-.0529	.0296	.0017
.00	-.1442	.0457	.0034

R = 0.72 × 10^6			
α, deg	C_N	C_A	C_m
20.00	0.2986	0.0001	0.0032
18.00	.2489	.0016	.0023
16.00	.2013	.0034	.0020
14.00	.1555	.0052	.0013
12.00	.1099	.0080	.0010
10.00	.0672	.0114	.0007
8.00	.0250	.0158	.0005
6.00	-.0168	.0213	.0007
4.00	-.0594	.0282	.0007
2.00	-.1043	.0357	.0008
.00	-.1472	.0447	.0017

(j) Model 10

R = 0.73 × 10^6			
α, deg	C_N	C_A	C_m
14.00	0.1788	0.0042	0.0062
12.00	.1409	.0039	.0062
10.00	.1045	.0053	.0045
9.00	.0891	.0059	.0040
8.00	.0710	.0054	.0040
6.00	.0430	.0064	.0027
4.00	.0182	.0091	.0017
2.00	-.0172	.0108	.0008
.00	-.0414	.0139	-.0005

R = 1.50 × 10^6			
α, deg	C_N	C_A	C_m
14.00	0.1766	0.0011	0.0053
12.00	.1353	.0016	.0045
10.00	.0995	.0024	.0039
8.00	.0664	.0029	.0029
6.00	.0364	.0040	.0025
4.00	.0095	.0057	.0013
2.00	-.0197	.0078	.0007
.00	-.0463	.0099	.0000

(k) Model 11

R = 0.64 × 10^6			
α, deg	C_N	C_A	C_m
14.00	0.1604	0.0078	0.0084
12.00	.1315	.0077	.0065
10.00	.0993	.0087	.0057
8.00	.0671	.0073	.0053
7.00	.0577	.0078	.0048
6.00	.0411	.0078	.0041
4.00	.0182	.0098	.0027
2.00	-.0033	.0088	.0007
.00	-.0250	.0116	-.0009

R = 1.36 × 10^6			
α, deg	C_N	C_A	C_m
14.00	0.1626	0.0039	0.0060
12.00	.1294	.0040	.0055
7.00	.0577	.0042	.0034
6.00	.0426	.0044	.0032
4.00	.0192	.0056	.0018
2.00	-.0031	.0062	.0002
.00	-.0245	.0075	-.0012

TABLE I.- TABULATION OF DATA - Continued

(l) Model 12

R = 0.67 × 10^6			
α, deg	C_N	C_A	C_m
14.00	0.1760	0.0008	0.0037
12.00	.1367	.0047	.0025
10.00	.1002	.0048	.0020
8.00	.0660	.0053	.0016
6.00	.0382	.0063	.0013
4.00	.0090	.0082	.0004
2.00	-.0181	.0100	-.0001
.00	-.0456	.0124	-.0007

R = 0.92 × 10^6			
α, deg	C_N	C_A	C_m
14.00	0.1767	0.0013	0.0042
12.00	.1381	.0038	.0032
10.00	.1013	.0040	.0031
8.00	.0656	.0044	.0016
6.00	.0370	.0057	.0018
4.00	.0087	.0076	.0012
2.00	-.0191	.0095	.0004
.00	-.0440	.0119	-.0009

(m) Model 13

R = 0.61 × 10^6			
α, deg	C_N	C_A	C_m
18.00	0.2922	0.0005	0.0052
16.00	.2412	.0028	.0032
14.00	.1902	.0040	.0028
12.00	.1465	.0049	.0020
10.00	.1050	.0069	.0016
8.00	.0667	.0091	.0019
6.00	.0255	.0115	.0004
4.00	-.0081	.0145	.0020
2.00	-.0394	.0187	-.0030

R = 0.67 × 10^6			
α, deg	C_N	C_A	C_m
18.00	0.2811	0.0018	0.0040
16.00	.2239	.0029	.0038
14.00	.1799	.0042	.0029
12.00	.1383	.0055	.0026
10.00	.0994	.0068	.0019
8.00	.0638	.0087	.0015
6.00	.0292	.0111	.0012
4.00	-.0092	.0136	.0004
2.00	-.0446	.0179	.0008
.00	-.0796	.0231	.0001

(n) Model 14

R = 0.61 × 10^6			
α, deg	C_N	C_A	C_m
18.00	0.2949	0.0036	-0.0008
16.00	.2399	.0056	-.0002
14.00	.1826	.0074	-.0014
12.00	.1306	.0103	-.0016
10.00	.0868	.0134	-.0017
8.00	.0407	.0174	-.0003
6.00	-.0015	.0226	-.0001
4.00	-.0390	.0291	-.0061

R = 0.65 × 10^6			
α, deg	C_N	C_A	C_m
18.00	0.2923	0.0028	0.0030
16.00	.2381	.0045	-.0019
14.00	.1843	.0066	-.0003
12.00	.1363	.0092	-.0001
10.00	.0868	.0121	-.0014
8.00	.0417	.0162	-.0016
6.00	.0001	.0208	.0007
4.00	-.0288	.0282	-.0102

TABLE I.- TABULATION OF DATA - Concluded

(o) Model 15

$R = 0.35 \times 10^6$			
α, deg	C_N	C_A	C_m
21.00	0.3491	0.0062	0.0082
19.00	.2895	.0088	.0065
16.00	.1977	.0140	.0058
14.00	.1444	.0182	.0022
12.00	.0966	.0243	.0023
10.00	.0348	.0326	-.0014
8.00	-.0194	.0412	-.0016
4.00	-.1240	.0653	-.0010
.00	-.2396	.0961	.0008

$R = 0.66 \times 10^6$			
α, deg	C_N	C_A	C_m
21.00	0.3411	0.0036	0.0090
19.00	.2793	.0060	.0074
16.00	.1867	.0107	.0052
14.00	.1347	.0163	.0049
12.00	.0845	.0223	.0021
10.00	.0278	.0313	.0050
8.00	-.0279	.0405	.0008

(p) Model 16

$R = 0.98 \times 10^6$			
α, deg	C_N	C_A	C_m
20.00	0.3111	0.0022	0.0032
18.00	.2632	.0045	.0027
16.00	.2015	.0079	.0024
14.00	.1503	.0123	.0023
12.00	.0979	.0179	.0031
10.00	.0472	.0246	.0034
8.00	-.0087	.0337	.0041
4.00	-.1108	.0535	.0059
.00	-.2190	.0803	.0092

$R = 1.50 \times 10^6$			
α, deg	C_N	C_A	C_m
20.00	0.3088	0.0029	0.0026
18.00	.2593	.0048	.0023
16.00	.1997	.0077	.0022
14.00	.1404	.0120	.0023
12.00	.0904	.0171	.0027
10.00	.0378	.0242	.0033
8.00	-.0173	.0326	.0038
6.00	-.0674	.0422	.0049
4.00	-.1260	.0546	.0061
2.00	-.1760	.0668	.0078
.00	-.2229	.0792	.0093

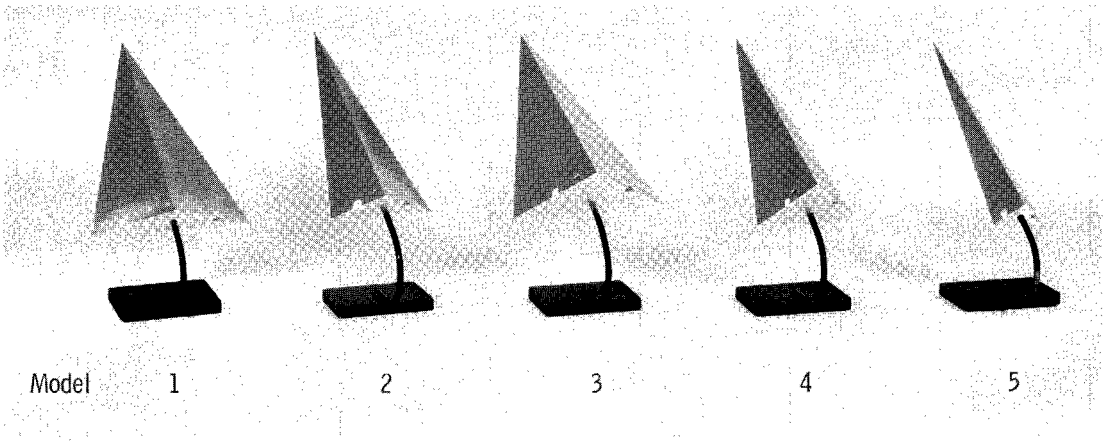

(a) Roof delta wings.

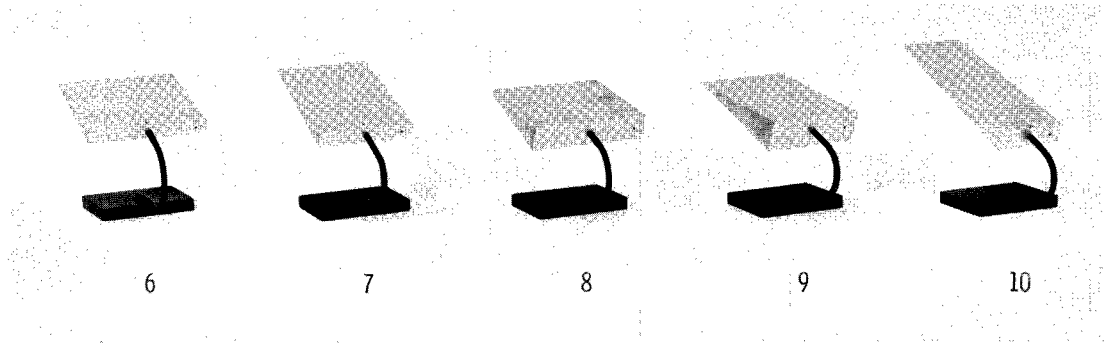

(b) Rectangular wings having aspect ratios and volume characteristics similar to delta wings shown in part (a).

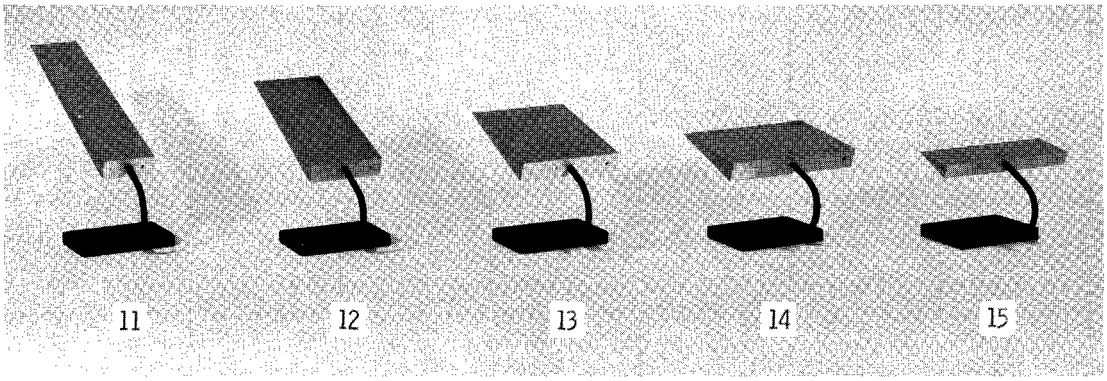

L-65-113

(c) Rectangular wings with various aspect ratios.

Figure 1.- Photographs of models.

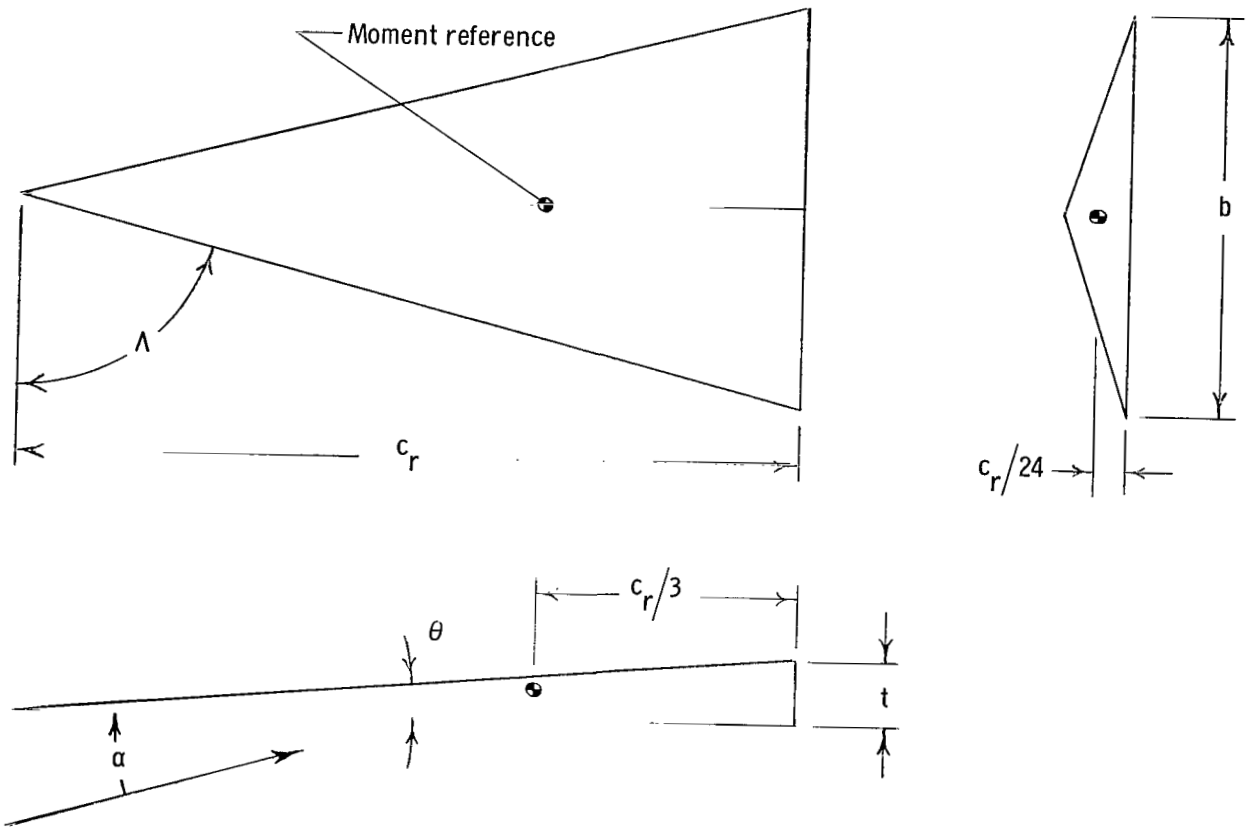

Model	θ, deg	Λ, deg	b, in.	c_r, in.	t, in.	S_p, in^2	S_b, in^2	V, in^3	$V^{2/3}/S_p$	t/c_r	A
1	5	75	6.431	12	1.050	38.59	3.376	13.5	0.147	0.088	1.07
2	5	80	4.231	12	1.050	25.49	2.221	8.9	.168	.088	.702
3	10	75	6.431	12	2.116	38.59	6.800	27.2	.234	.176	1.07
4	10	80	4.231	12	2.116	25.49	4.475	17.9	.268	.176	.702
5	5	85	2.100	12	1.050	12.60	1.103	4.4	.210	.088	.35

(a) Roof delta wing.

Figure 2.- Detail dimensions of models.

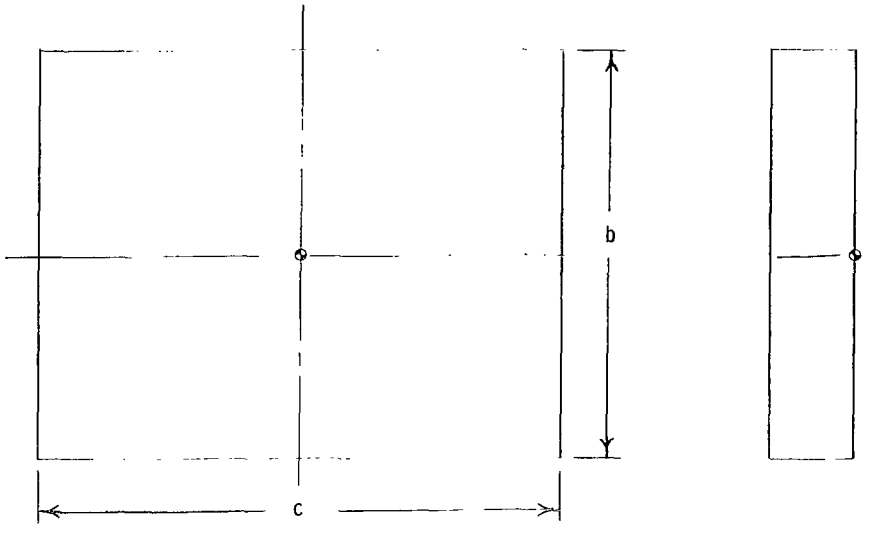

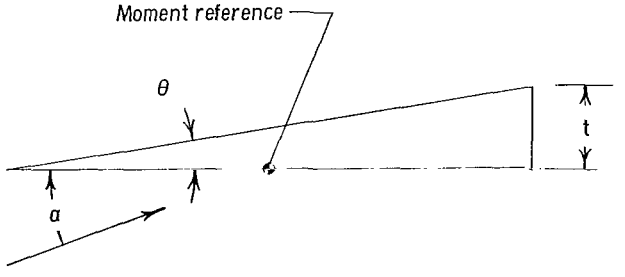

Model	θ, deg	b, in.	c, in.	t, in.	S_p, in^2	S_b, in^2	V, in^3	$V^{2/3}/S_p$	t/c	A
6	6.63	5.070	4.734	0.551	24.0	2.79	6.612	0.147	0.116	1.07
7	6.58	4.105	5.846	.675	24.0	2.77	8.099	.168	.115	.702
8	13.18	5.070	4.734	1.108	24.0	5.62	13.293	.234	.234	1.07
9	13.15	4.105	5.846	1.366	24.0	5.61	16.386	.268	.234	.702
10	6.37	2.899	8.290	.923	24.0	2.68	11.084	.210	.111	.35
11	4.57	2.191	10.954	.876	24.0	1.92	10.505	.200	.08	.20
12	6.45	3.098	7.745	.876	24.0	2.71	10.502	.200	.11	.40
13	9.08	4.382	5.478	.876	24.0	3.84	10.512	.200	.16	.80
14	12.35	6.000	4.000	.876	24.0	5.26	10.512	.200	.22	1.50
15	17.22	6.000	2.000	.620	12.0	3.72	3.72	.200	.31	3.00
16	16.70	4.899	4.899	1.470	24.0	7.20	17.600	.283	.30	1.00

(b) Rectangular wings.

Figure 2.- Concluded.

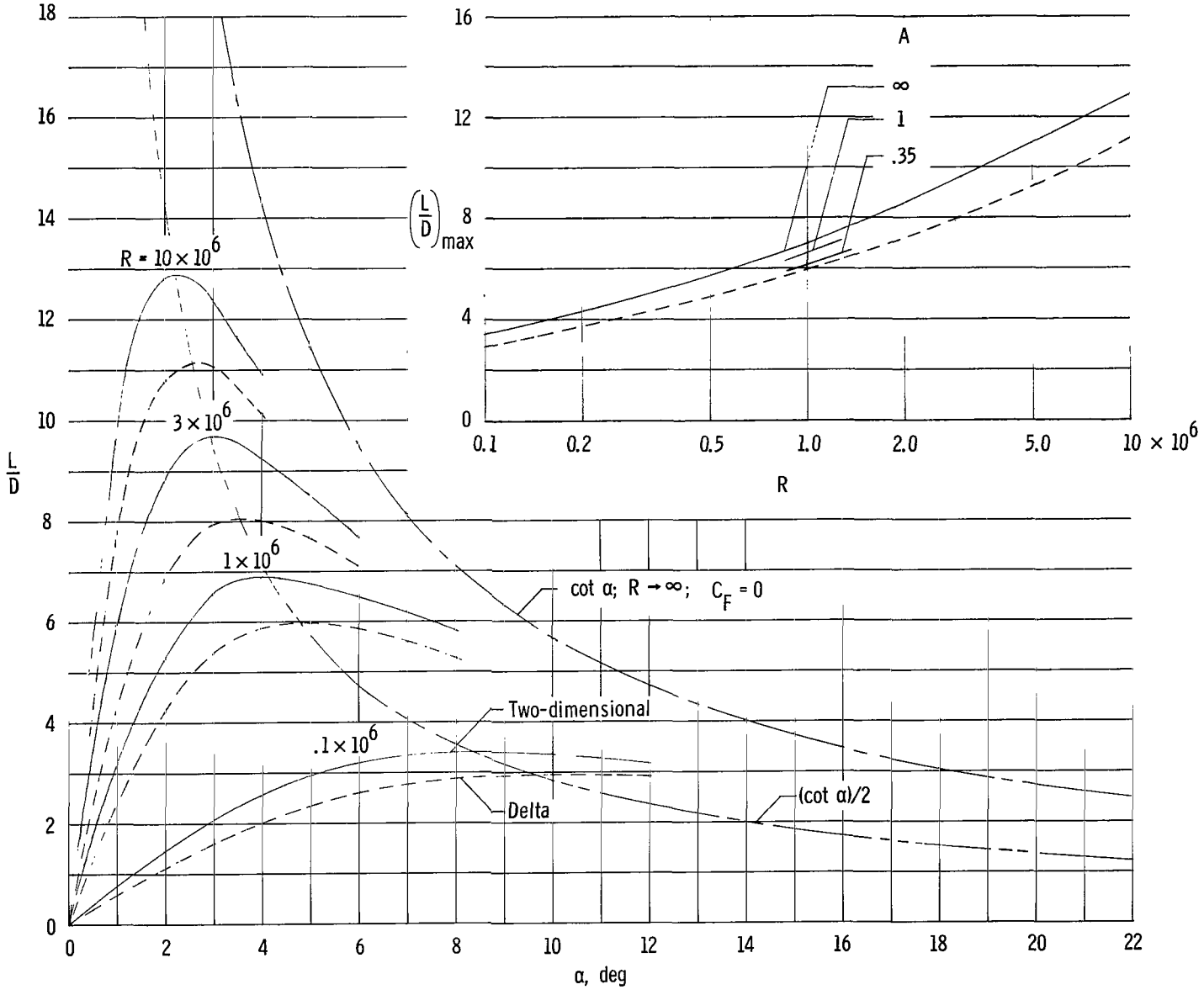

Figure 3.- Theoretical effect of Reynolds number variation on lift-drag ratio of zero-thickness flat-plate two-dimensional and delta-planform wings. M = 6.9.

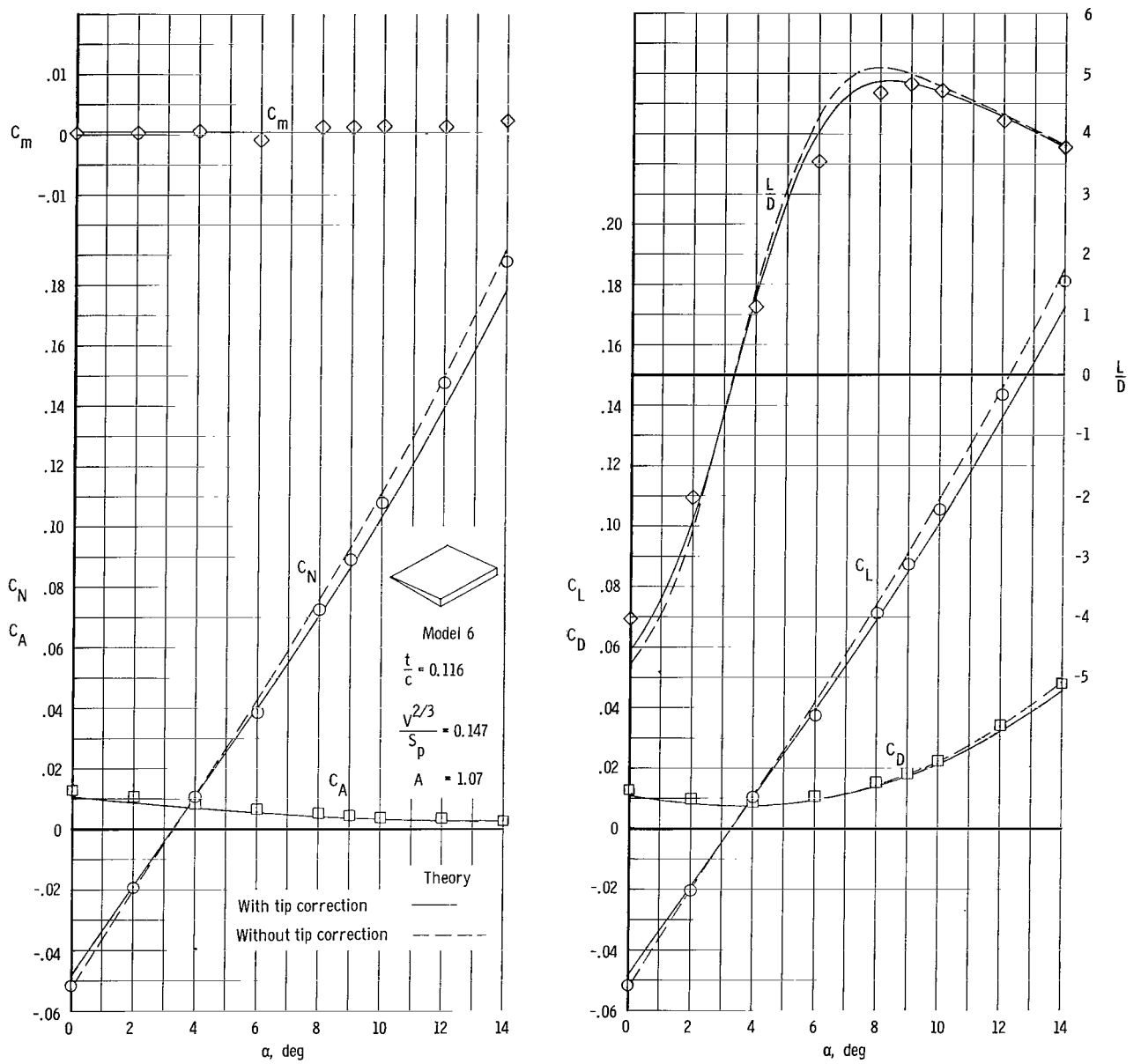

(a) Rectangular wedge. $R = 0.68 \times 10^6$.

Figure 4.- Comparison of theory and experiment. M = 6.9.

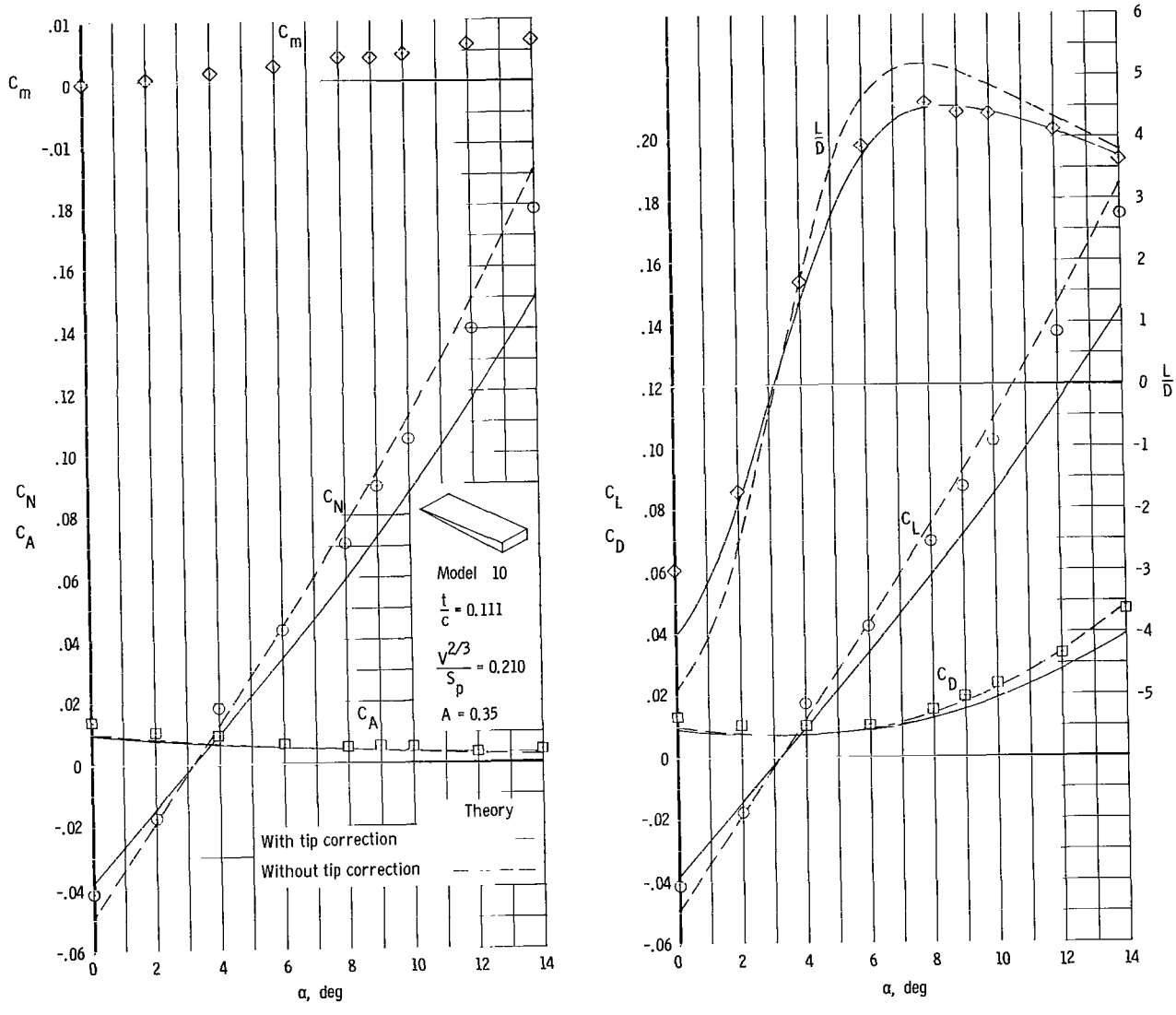

(b) Rectangular wedge. $R = 0.73 \times 10^6$.

Figure 4.- Continued.

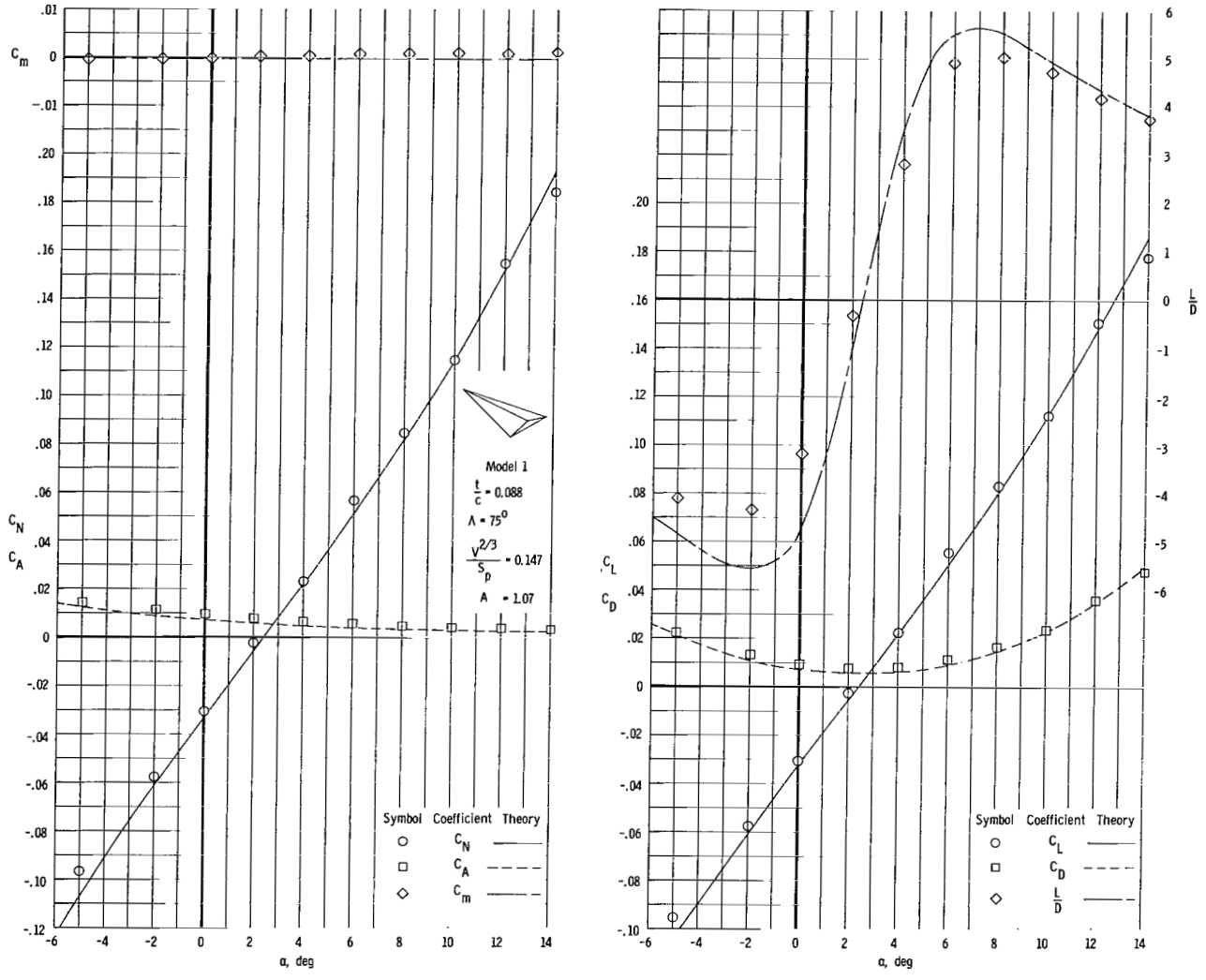

(c) Roof delta wing. R = 1.36×10^6.

Figure 4.- Continued.

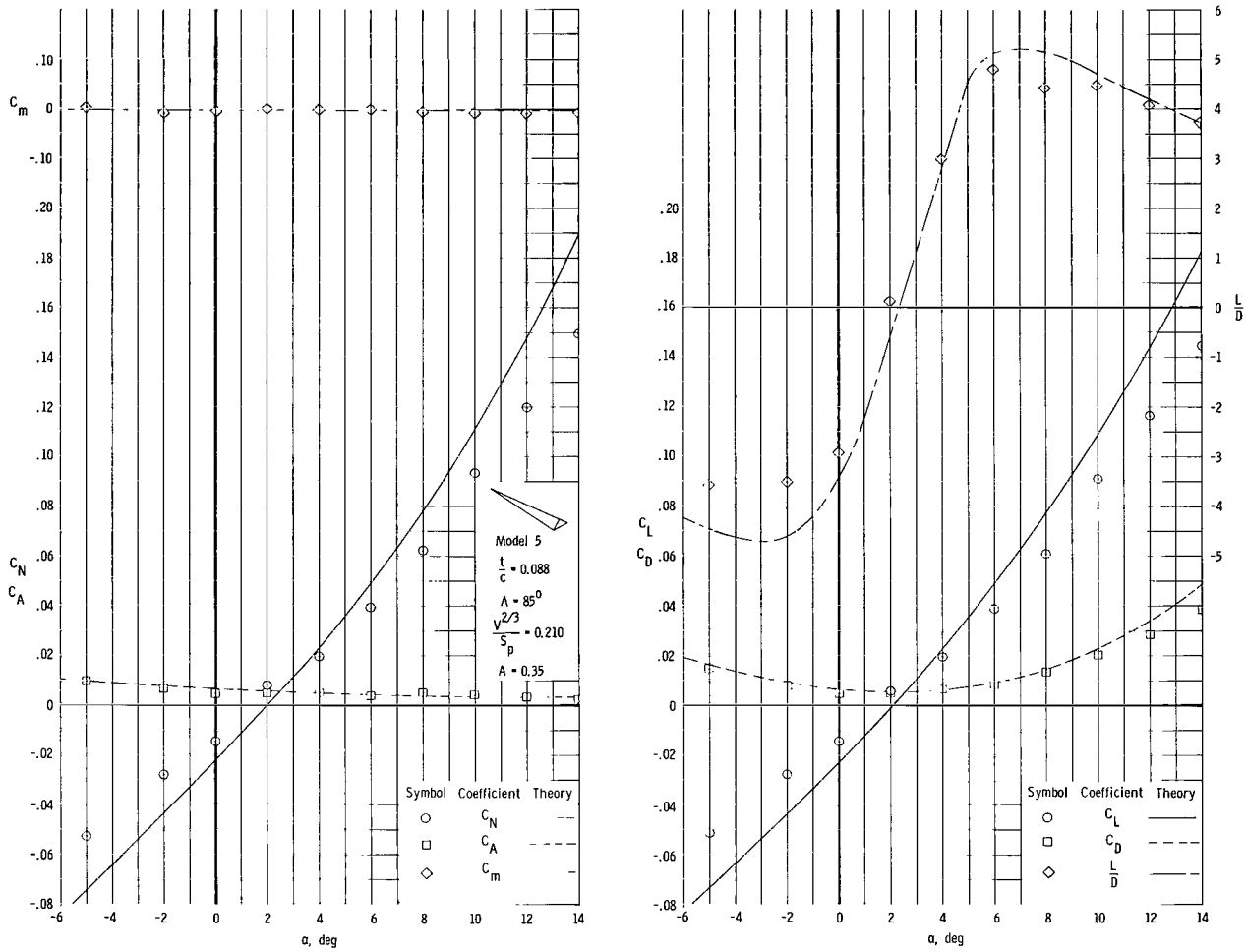

(d) Roof delta wing. $R = 1.38 \times 10^6$.

Figure 4.- Concluded.

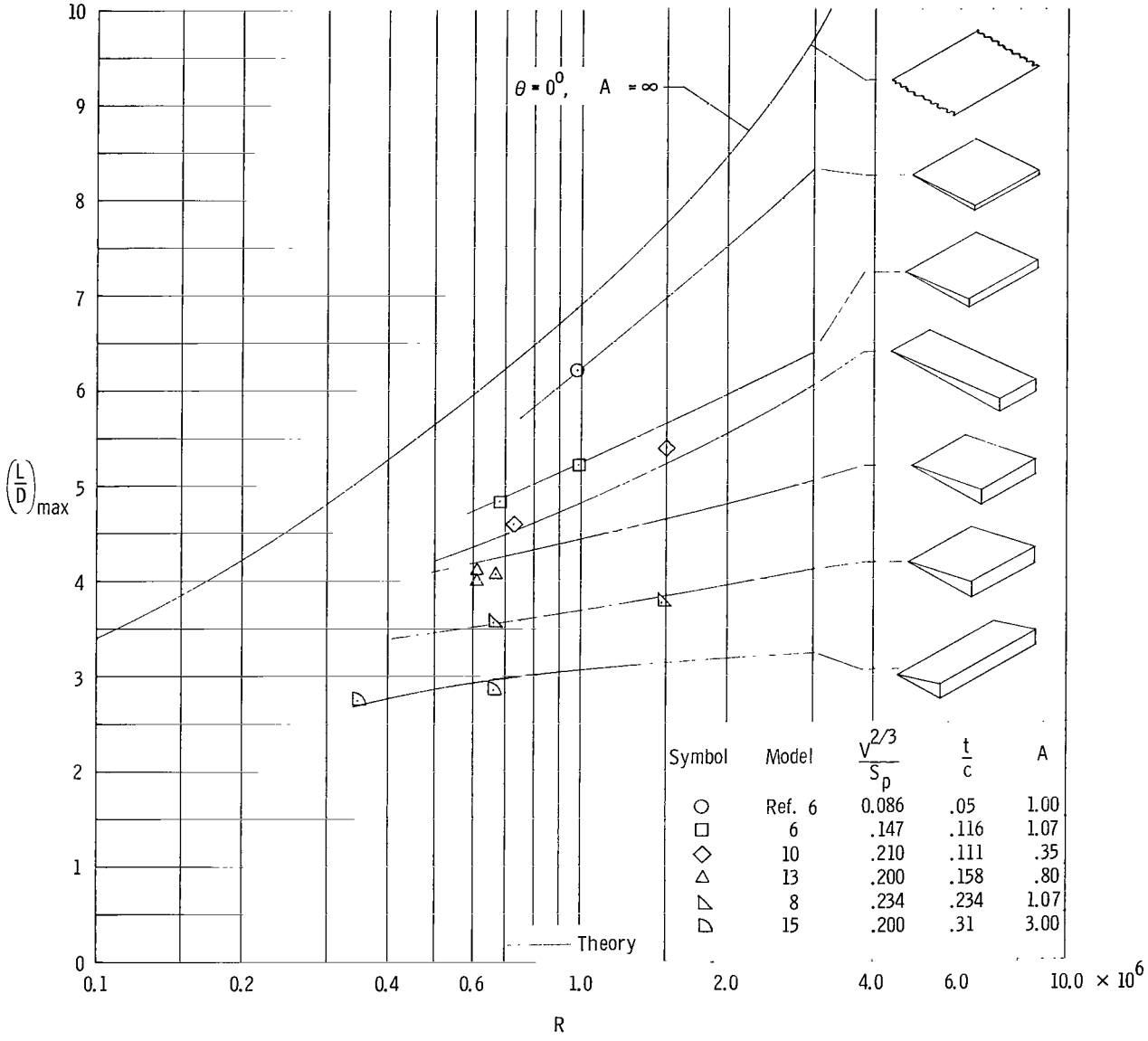

(a) Rectangular wings.

Figure 5.- Effect of Reynolds number on $(L/D)_{max}$. M = 6.9.

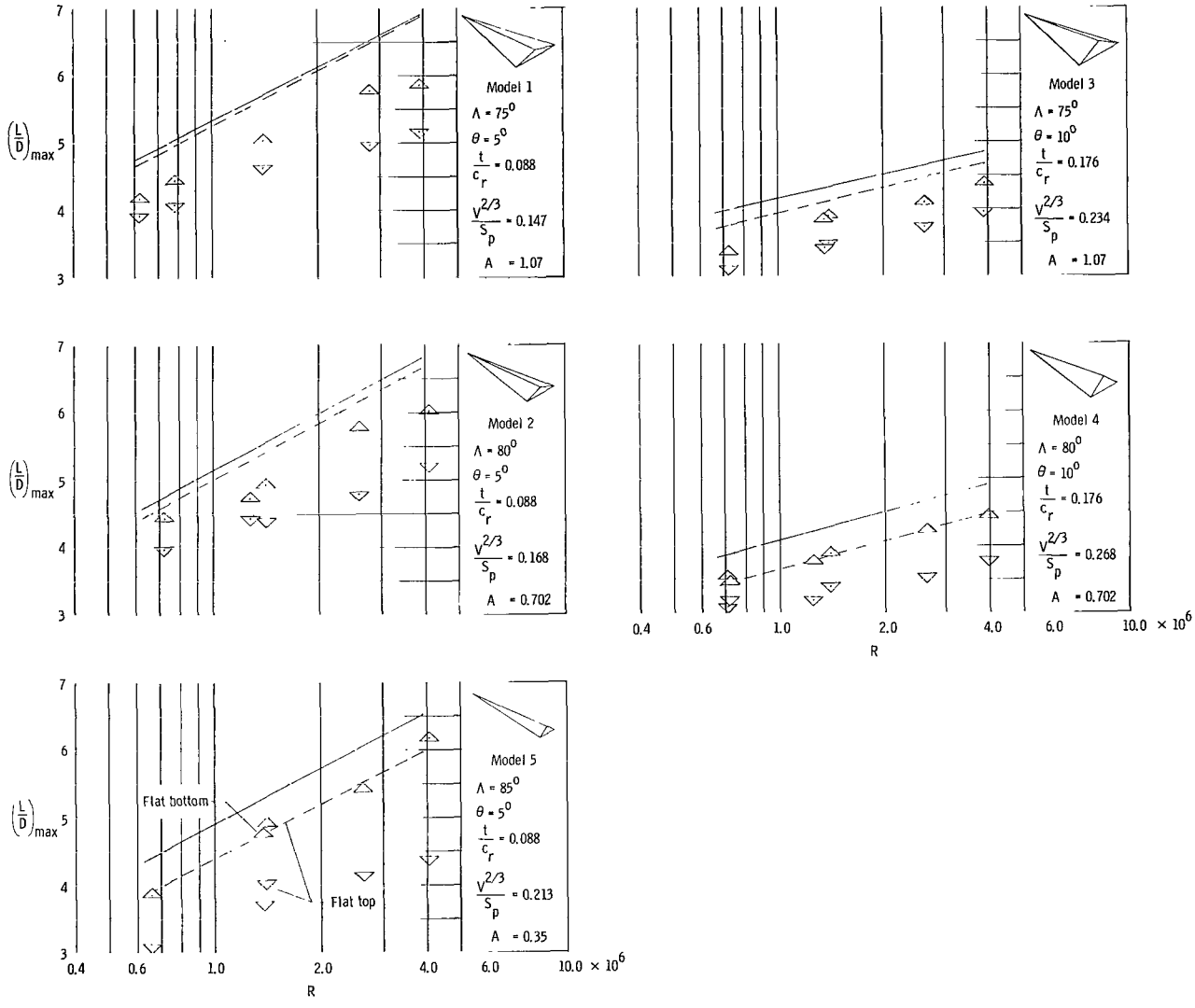

(b) Roof delta wings.

Figure 5.- Concluded.

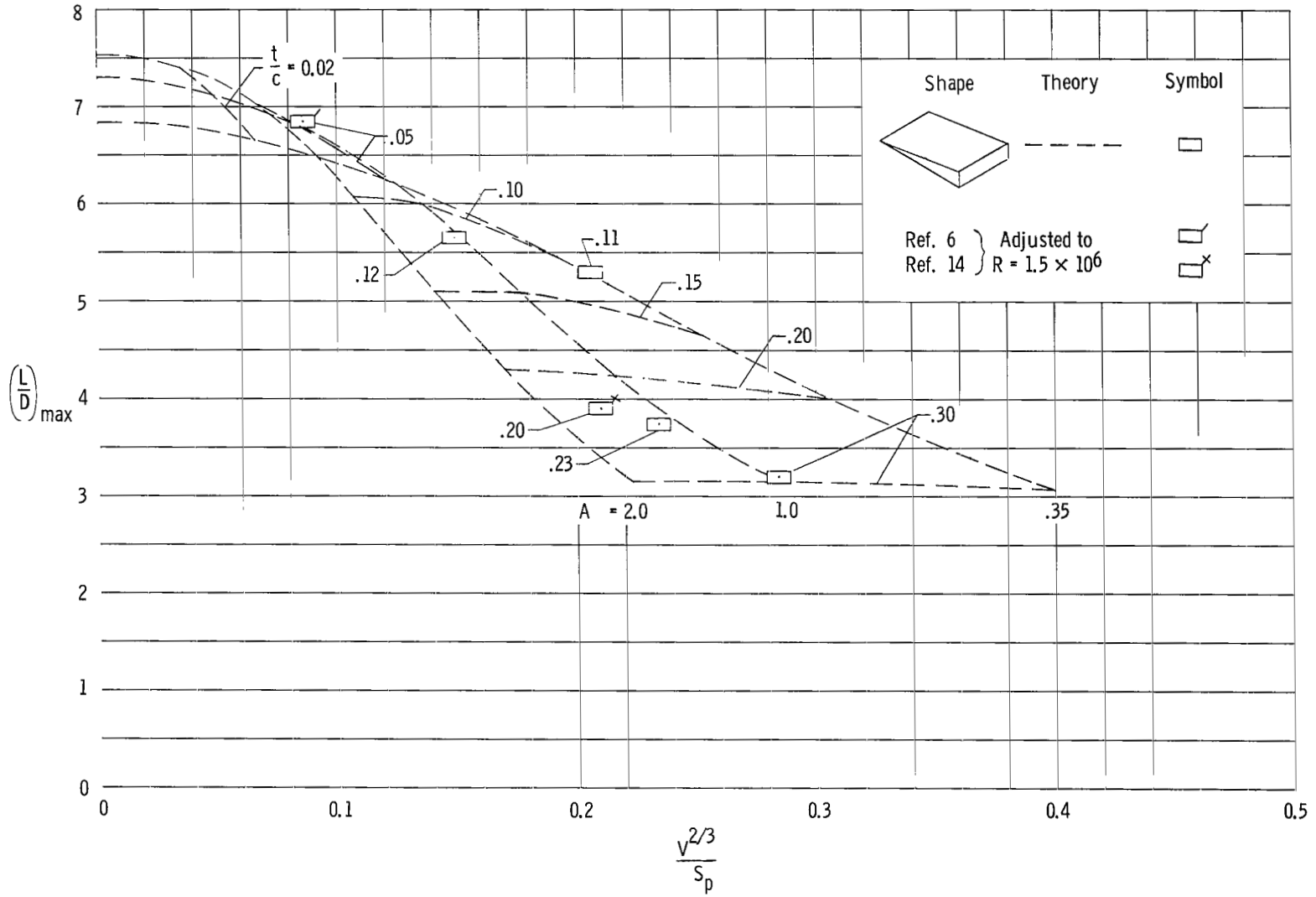

(a) Rectangular wings.

Figure 6.- Variation of $(L/D)_{max}$ with volume ratio. R = 1.5 × 10^6; M = 6.9.

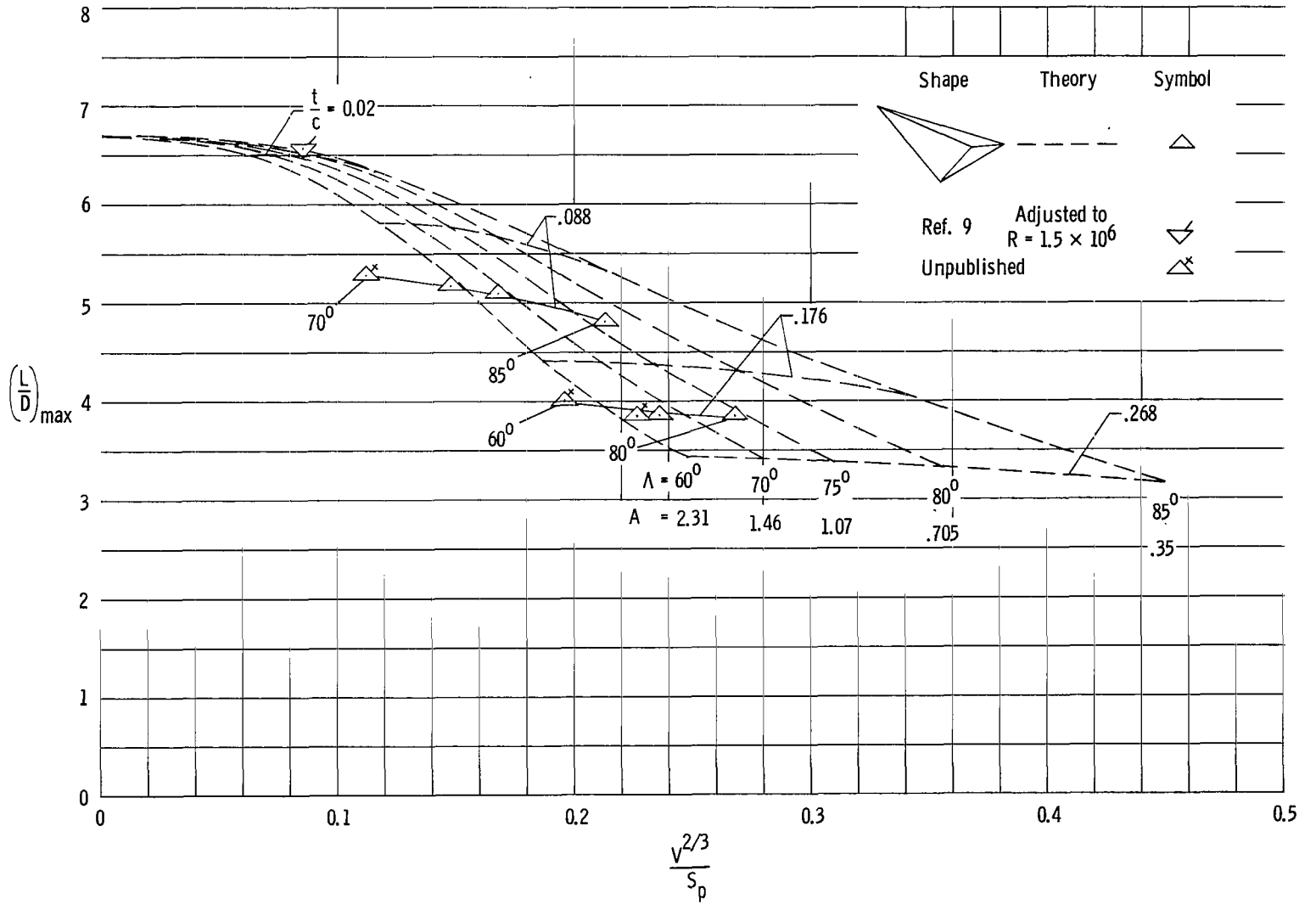

(b) Roof delta wings.

Figure 6.- Concluded.

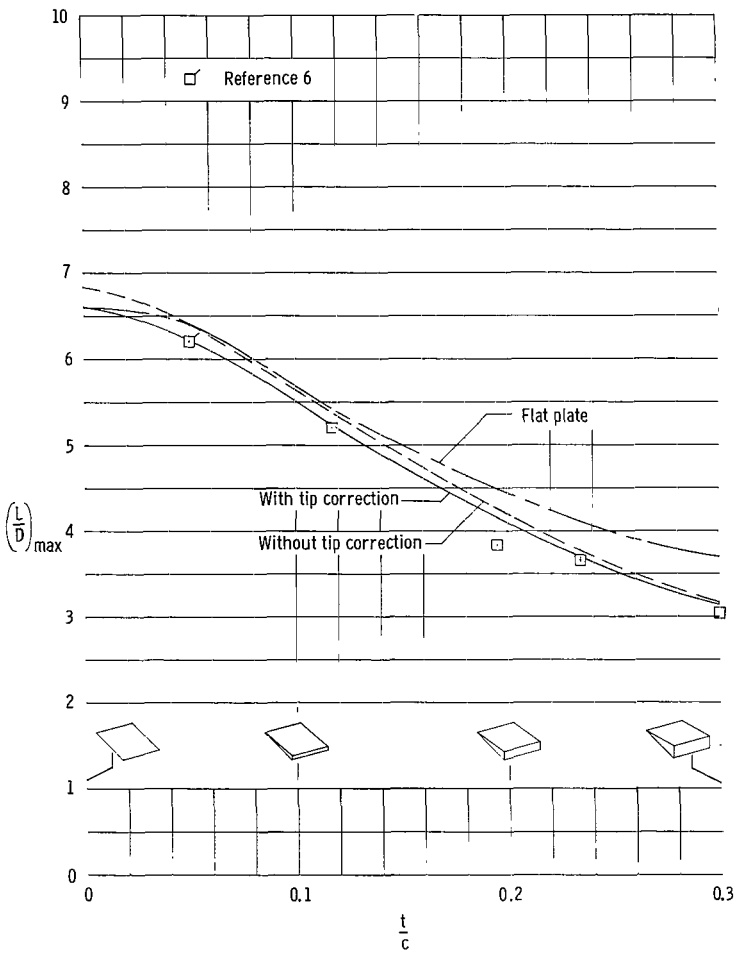

(a) Rectangular wings. $R = 0.98 \times 10^6$; $A = 1.00$.

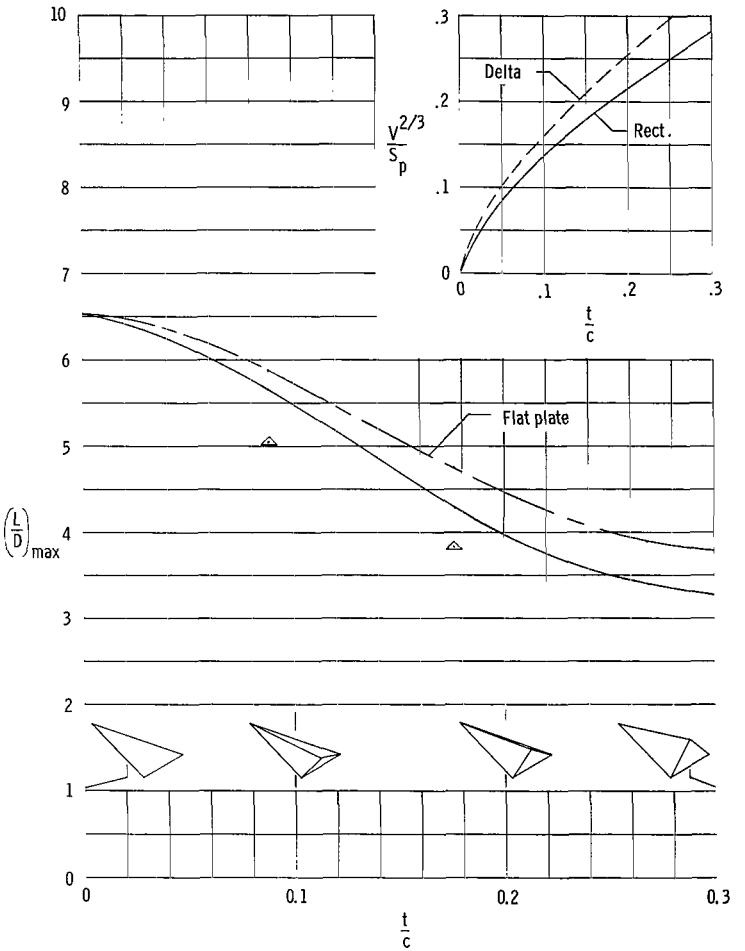

(b) Delta wings. $R = 1.33 \times 10^6$; $A = 1.07$.

Figure 7.- Variation of $(L/D)_{max}$ with thickness ratio for rectangular and delta wings. $M = 6.9$.

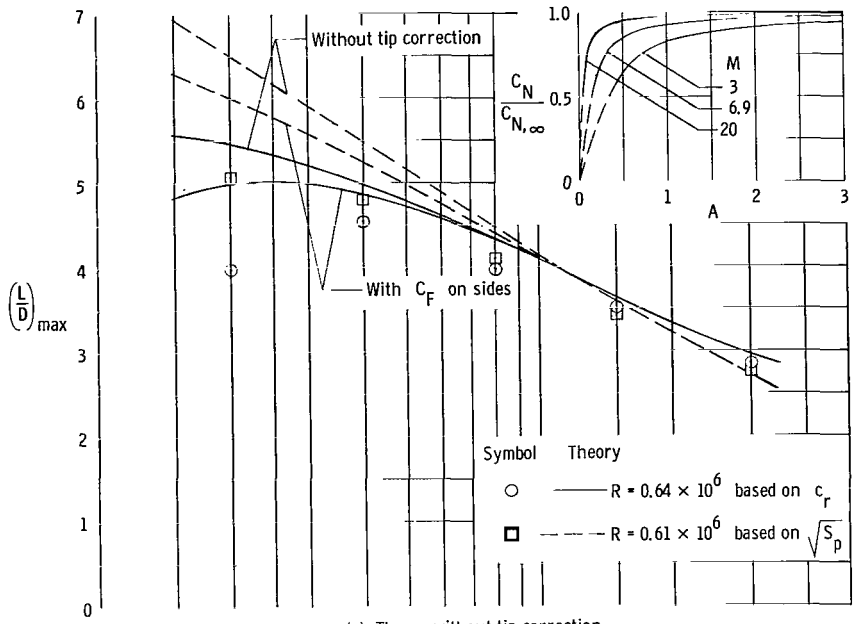

(a) Theory without tip correction.

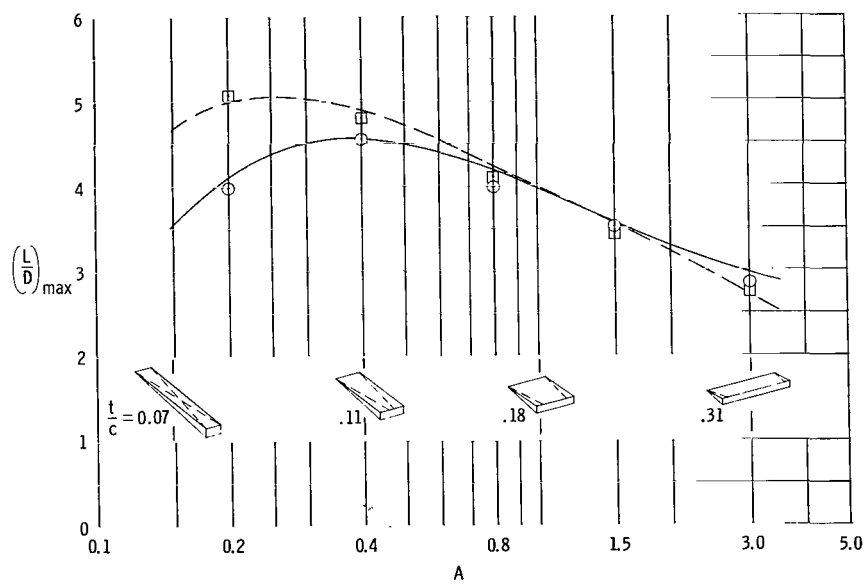

(b) Theory with tip correction.

Figure 8.- Variation of $(L/D)_{max}$ with aspect ratio for rectangular two-dimensional wedges. $\frac{V^{2/3}}{S_p} = 0.20$; M = 6.9.

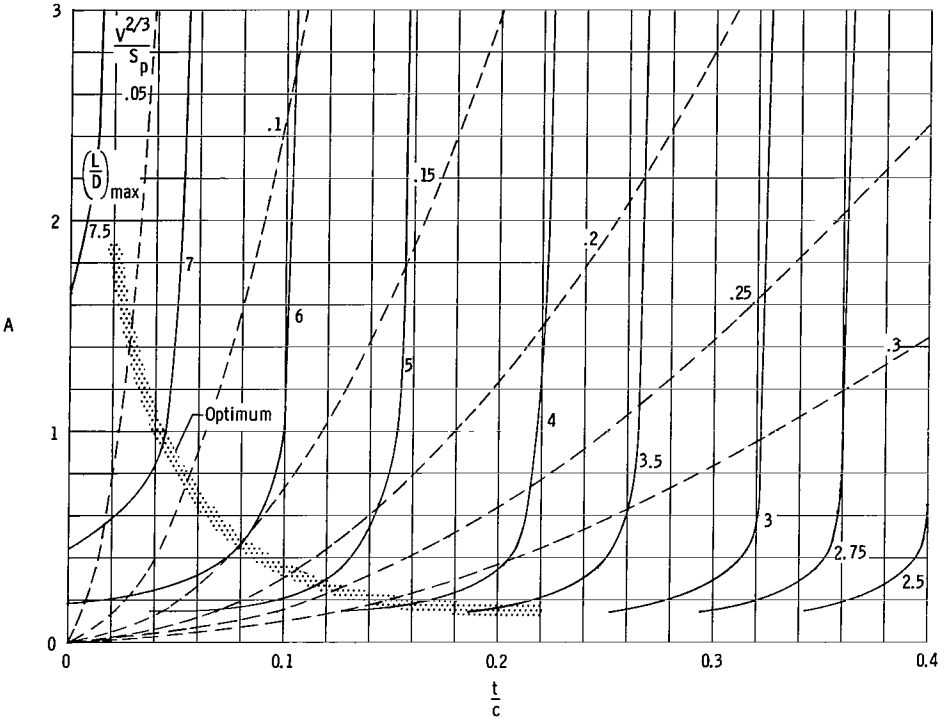

(a) Rectangular wings.

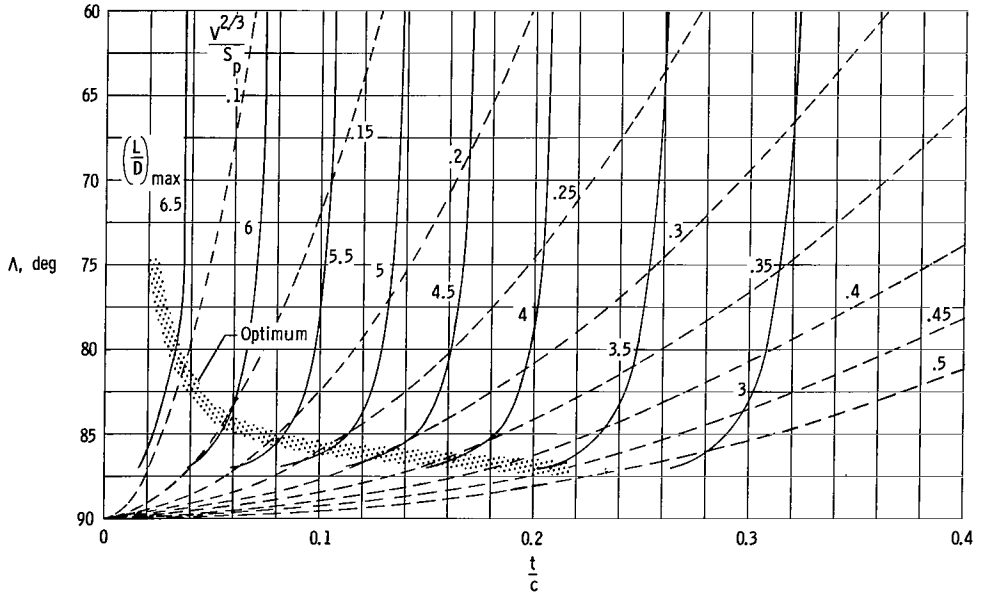

(b) Flat-bottom delta wings.

Figure 9.- Summary of theoretical wing characteristics and optimum configurations for $M = 6.9$ and $R = 1.5 \times 10^6$.

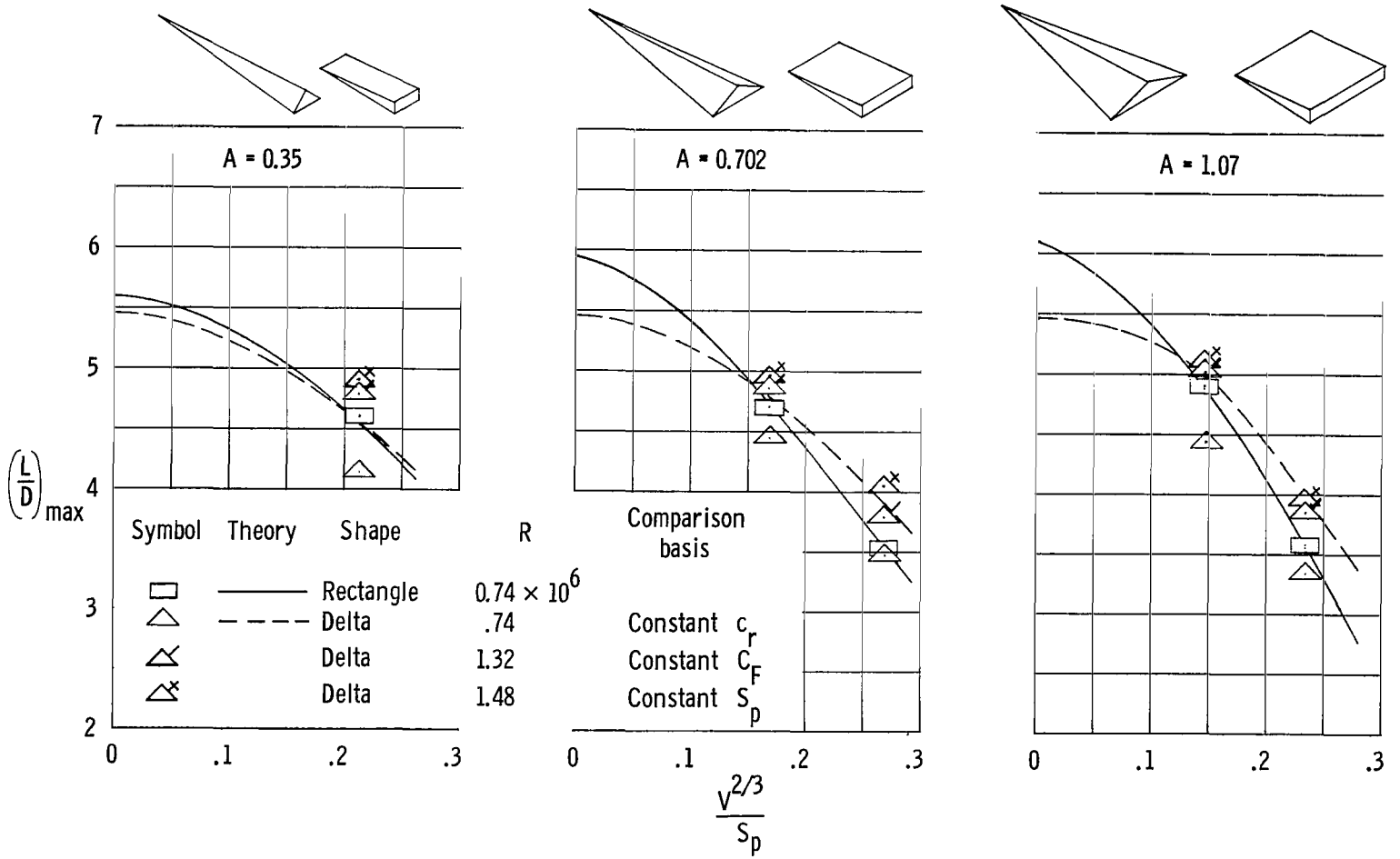

Figure 10.- Comparison of delta and rectangular planform wedges for constant values of $\frac{V^{2/3}}{S_p}$ and A. M = 6.9.

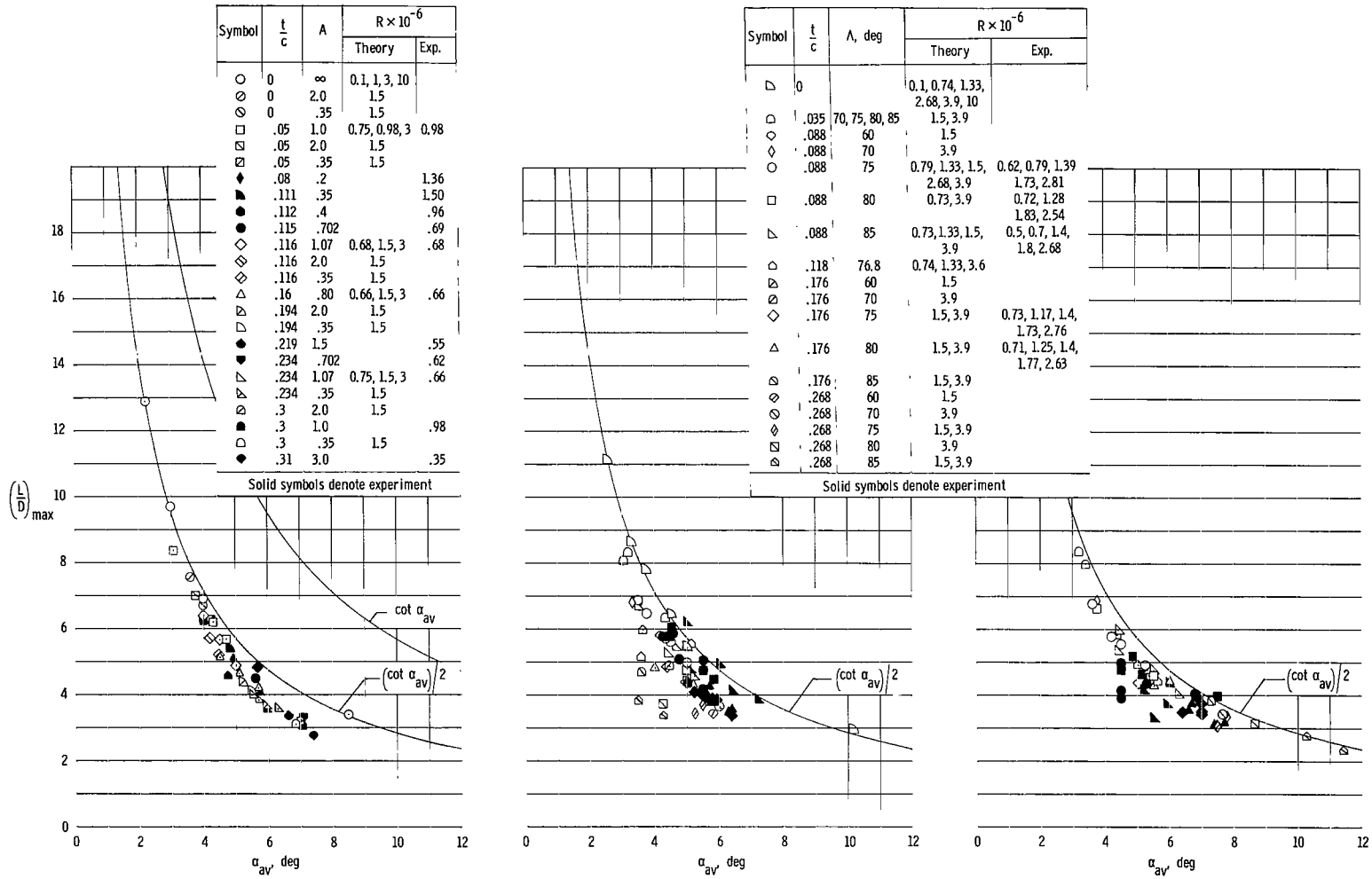

(a) Rectangular wings. (b) Flat-bottom delta wings. (c) Flat-top delta wings.

Figure 11.- Correlation of maximum lift-drag ratio of rectangular and delta planform wings with angle of attack. M = 6.9.

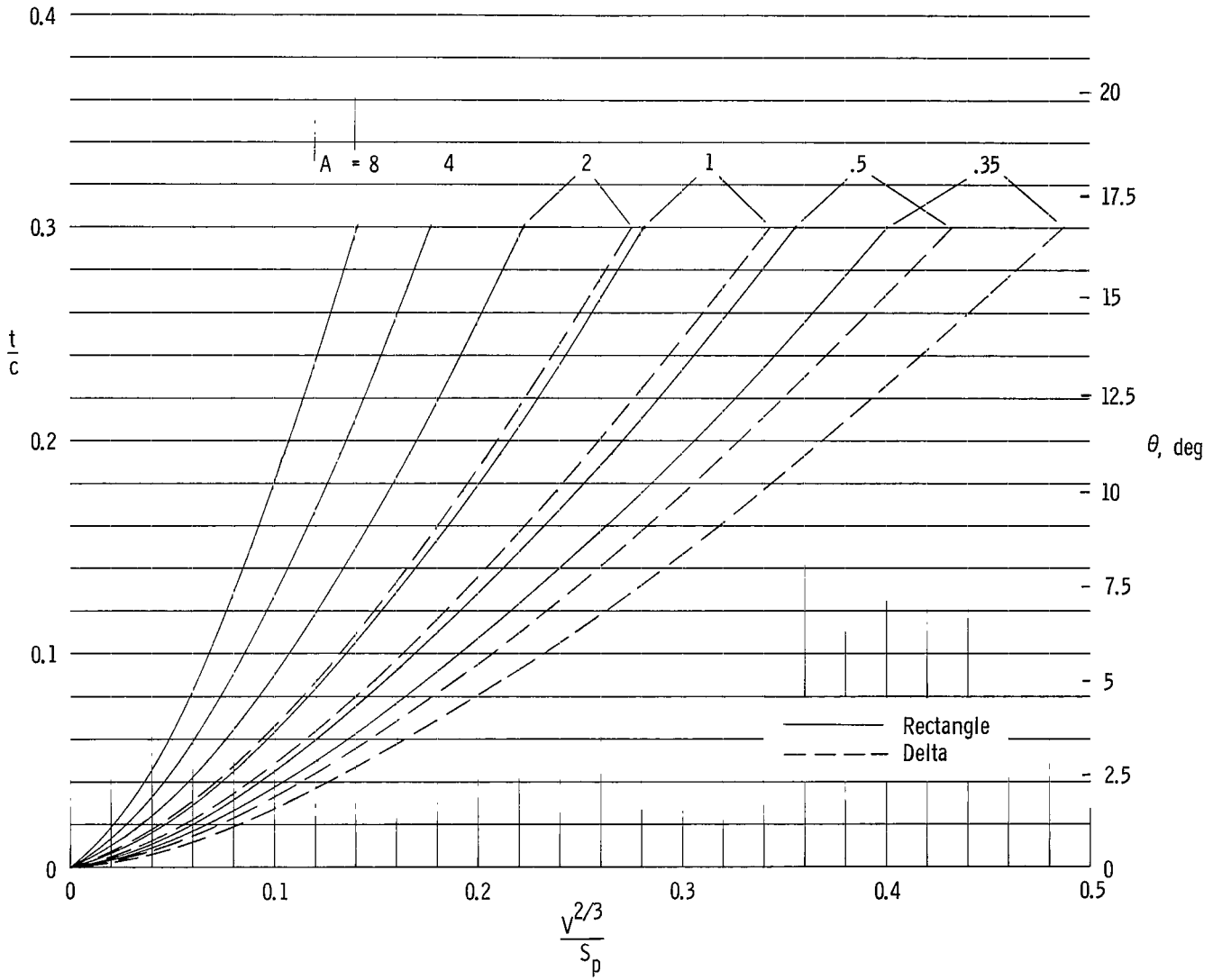

(a) Effect of A on $\frac{V^{2/3}}{S_p}$ for various t/c values.

Figure 12.- Geometry of rectangular and delta wedge wings.

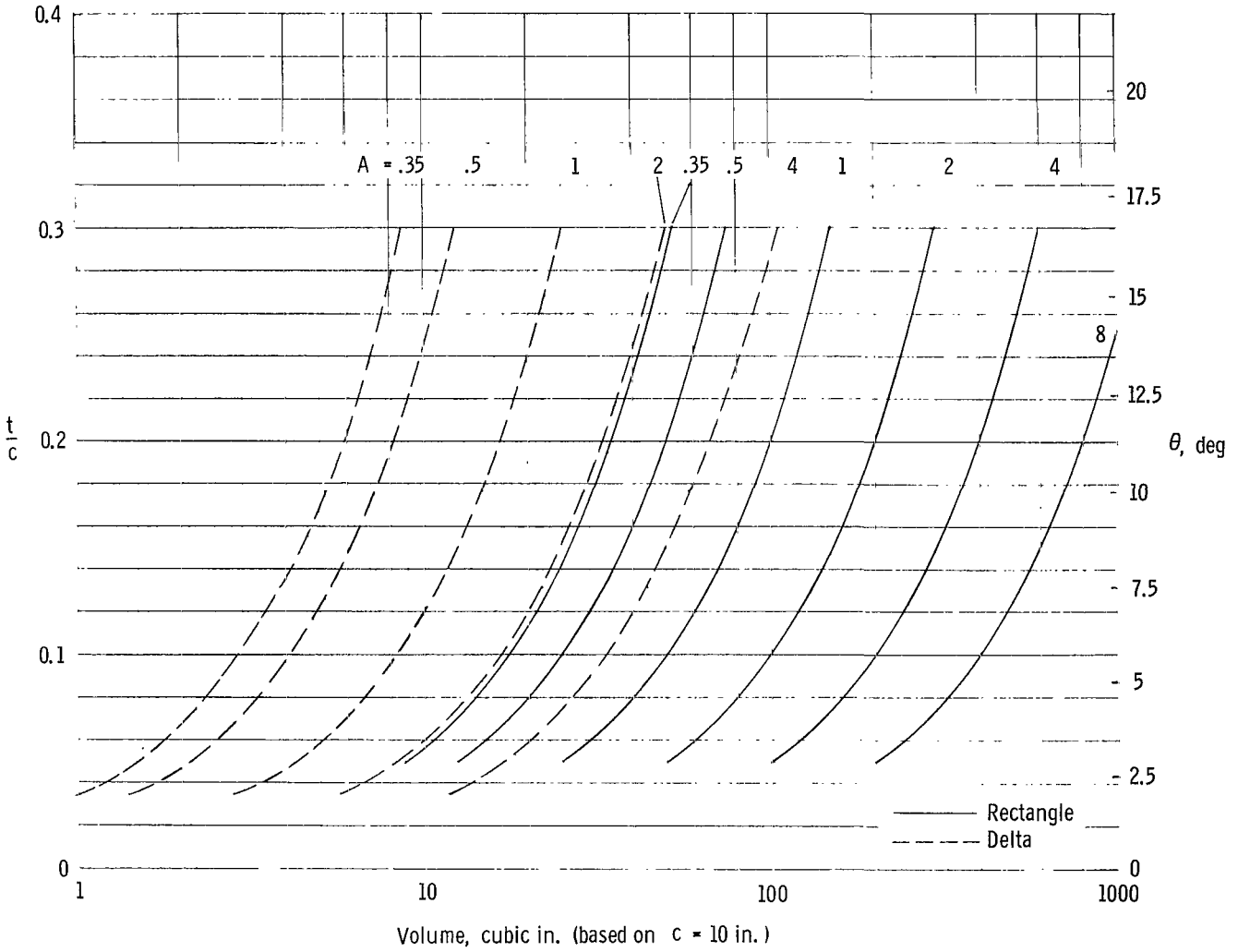

(b) Effect of A on V for various t/c values.

Figure 12.- Continued.

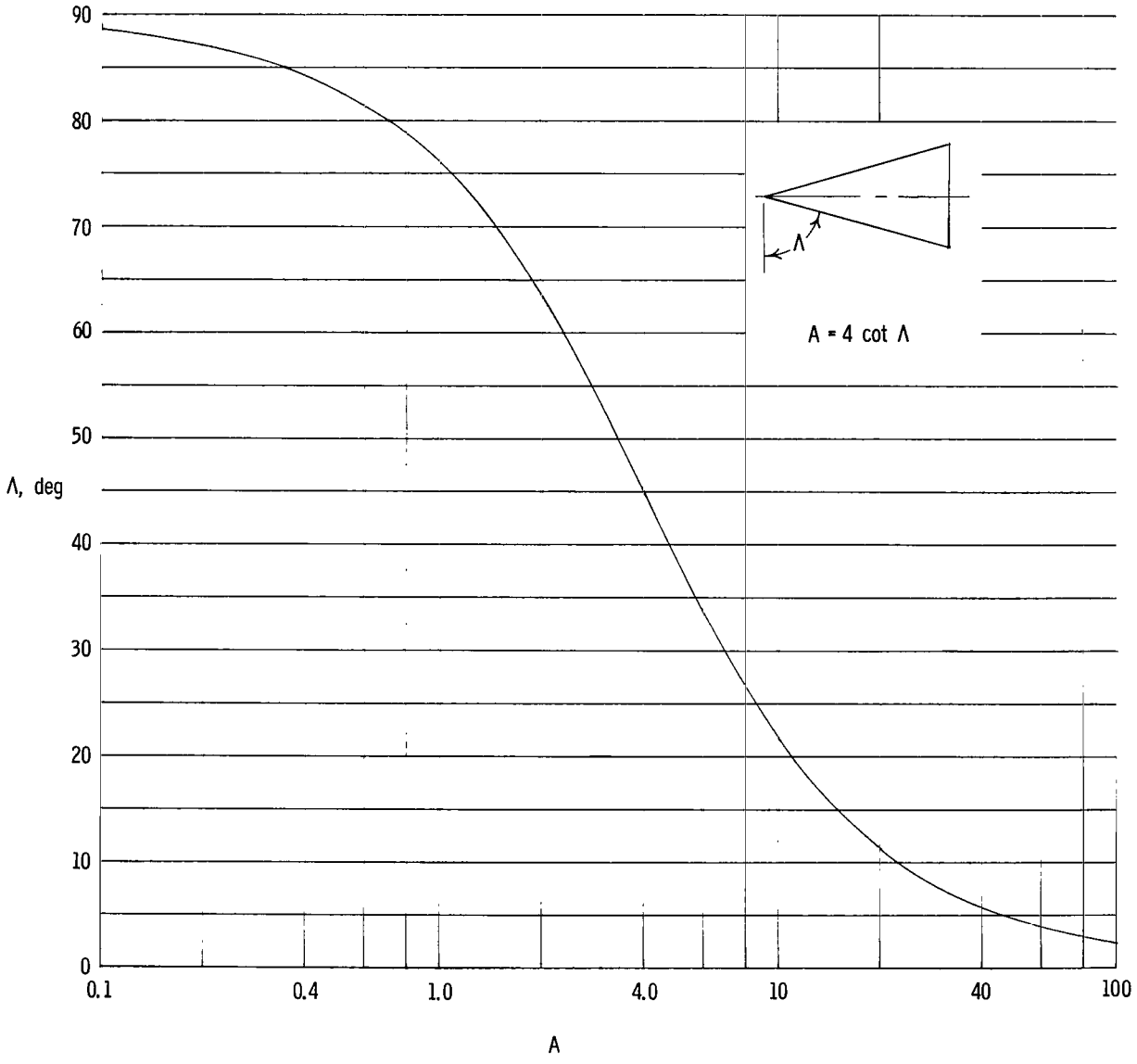

(c) Sweep angle plotted against A for delta wings.

Figure 12.- Concluded.

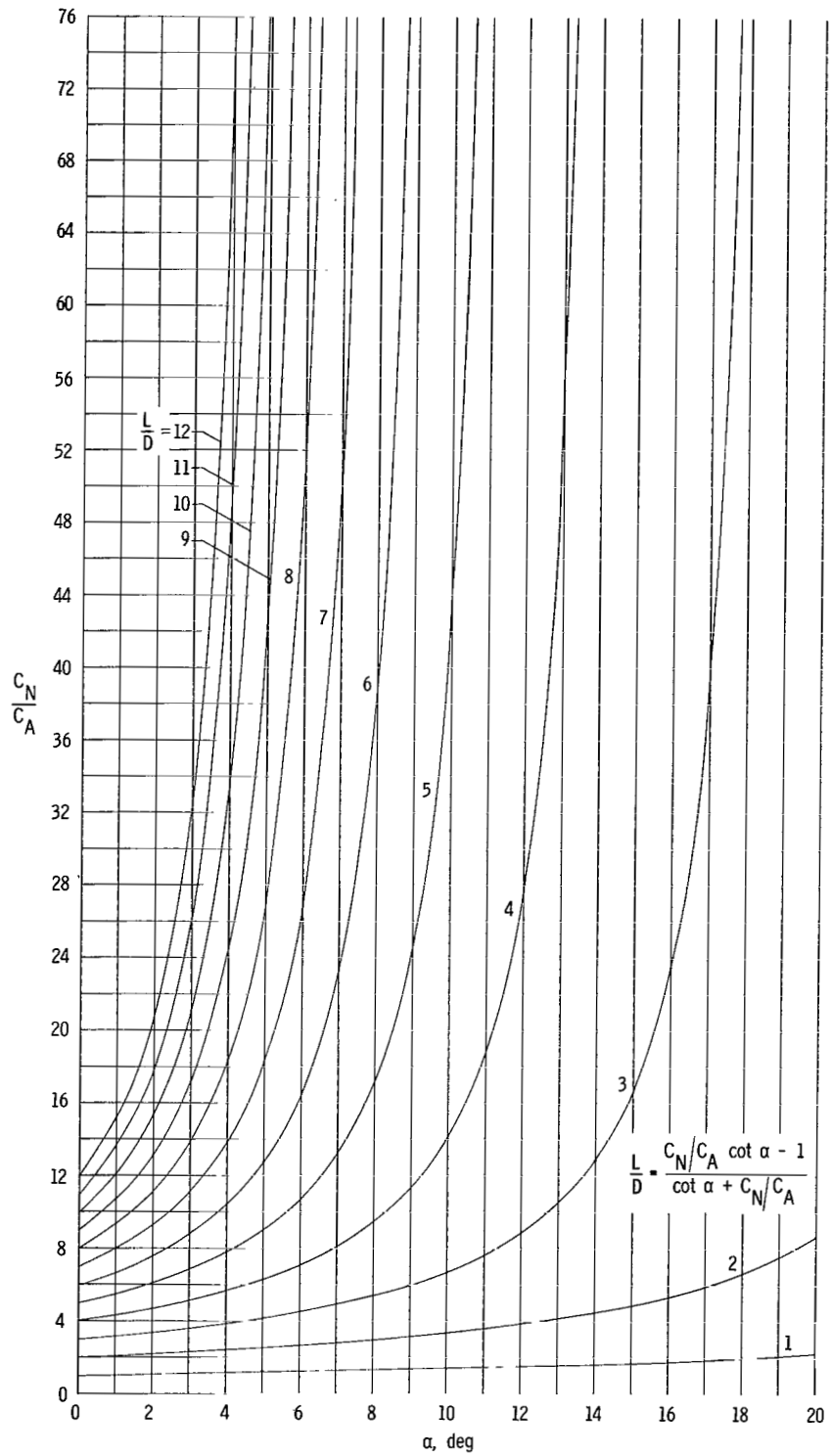

Figure 13.- Relation of normal-to-axial-force ratio, lift-drag ratio, and angle of attack.

NASA-Langley, 1965 L-4433

2-1-22-18

"The aeronautical and space activities of the United States shall be conducted so as to contribute . . . to the expansion of human knowledge of phenomena in the atmosphere and space. The Administration shall provide for the widest practicable and appropriate dissemination of information concerning its activities and the results thereof."

—NATIONAL AERONAUTICS AND SPACE ACT OF 1958

NASA SCIENTIFIC AND TECHNICAL PUBLICATIONS

TECHNICAL REPORTS: Scientific and technical information considered important, complete, and a lasting contribution to existing knowledge.

TECHNICAL NOTES: Information less broad in scope but nevertheless of importance as a contribution to existing knowledge.

TECHNICAL MEMORANDUMS: Information receiving limited distribution because of preliminary data, security classification, or other reasons.

CONTRACTOR REPORTS: Technical information generated in connection with a NASA contract or grant and released under NASA auspices.

TECHNICAL TRANSLATIONS: Information published in a foreign language considered to merit NASA distribution in English.

TECHNICAL REPRINTS: Information derived from NASA activities and initially published in the form of journal articles.

SPECIAL PUBLICATIONS: Information derived from or of value to NASA activities but not necessarily reporting the results of individual NASA-programmed scientific efforts. Publications include conference proceedings, monographs, data compilations, handbooks, sourcebooks, and special bibliographies.

Details on the availability of these publications may be obtained from:

SCIENTIFIC AND TECHNICAL INFORMATION DIVISION

NATIONAL AERONAUTICS AND SPACE ADMINISTRATION

Washington, D.C. 20546